

1

2 **Dynamic and thermodynamic contribution to the October 2019 exceptional**  
3 **rainfall in West Central Africa**

4

5 **Kevin Kenfack<sup>1\*</sup> · Francesco Marra<sup>3</sup> · Zéphirin Yepdo Djomou<sup>1,2</sup> · Lucie A. Djiotang**  
6 **Tchotchou<sup>1</sup> · Alain T. Tamoffo<sup>4</sup> · Derbetini A. Vondou<sup>1</sup>**

7

8 <sup>1</sup>Laboratory for Environmental Modelling and Atmospheric Physics (LEMAP), Physics Department,  
9 University of Yaoundé 1, Yaoundé, Cameroon

10 <sup>2</sup>National Institute of Cartography, Cameroon

11 <sup>3</sup>Department of Geosciences, University of Padova, Italy

12 <sup>4</sup>Climate Service Center Germany (GERICS), Helmholtz-Zentrum Hereon, Fischertwiete 1, 20095  
13 Hamburg, Germany

14

15

16 Corresponding author: **Kevin Kenfack**

17 Email: **kevinkenfack46@gmail.com**

18 ORCID: **0000-0003-1694-4906**

19 Kevin Kenfack's ORCID: 0000-0003-1694-4906

20 Francesco Marra's ORCID: 0000-0003-0573-9202

21 Lucie A. Djiotang Tchotchou's ORCID: 0000-0003-2860-428X

22 Alain T. Tamoffo's ORCID: 0000-0001-8482-8881

23 Derbetini A. Vondou's ORCID: 0000-0002-8681-5328

24

25 **Abstract**

26 Exceptional rainfall hit West Central Africa in October 2019. To understand the underlying  
27 mechanisms, we diagnosed the regional moisture and Moist Static Energy (MSE) budgets intending  
28 to highlight with a view to highlighting the importance of the dynamic and thermodynamic effects  
29 associated with this historic event. Analysis of the moisture budget reveals that the precipitation  
30 anomalies in October were mainly controlled by dynamic effects. (72.5% of the sum of dynamic and

31 ~~thermodynamic contributions~~)-Horizontal moisture advection induced by horizontal wind anomalies  
32 controls extreme precipitation north of West Central Africa, while vertical moisture advection  
33 induced by vertical velocity anomalies controls extreme precipitation south of West Central Africa.  
34 Changes in the thermodynamic effect, although not the key factor responsible for the events of  
35 October 2019, contribute up to 3527.5% of the total effect on the northern part and 15% on the  
36 southern part of the domain. The residual term (6°N-14°N, 6°-20°E) is important and provides a  
37 caveat when estimating dynamic and thermodynamic processes..-Diagnosis of the MSE balance  
38 averaged over the northern part of west Central Africa shows that the anomalous vertical motion is  
39 dominated by the dynamic effect, i.e. the wet enthalpy advection induced by the horizontal wind  
40 anomalies. This is confirmed by the high correlation (r = 0.6) between the two terms compared to the  
41 other terms. Whereas to the west of the Congo Basin, the increase in the net energy balance  
42 dominated the changes in vertical motion (r = 0.51). The horizontal advection of the MSE induced  
43 by the ~~anomaliesvariation~~ of the wet enthalpy and the vertical advection of the MSE induced by the  
44 ~~anomaliesvariation~~ of the MSE seem less important (r= 0.29 and -0.19 to the north and -0.17 and  
45 0.03 to the south respectively). ~~The strong anomalies~~.-~~The variations~~ in the MSE balance in the north  
46 are linked to its meridional component, in particular the meridional wind anomalies in the dynamic  
47 effect and the meridional ~~anomaliesvariations~~ in latent heat in the thermodynamic effect.~~This is due~~  
48 ~~to the increase in sea surface temperatures in the equatorial Atlantic, associated with the anomalous~~  
49 ~~thermal depression over the Sahara, which has increased rainfall over West Central Africa.~~ Our  
50 results suggest that dynamic and thermodynamic effects should be jointly considered for adequately  
51 anticipating this kind of extreme event. Understanding the associated mechanisms could help us  
52 improve our projections and increase the region's population resilience to these extreme weather  
53 events.

54 **Keywords:** West Central Africa · Moisture budget · Moist static energy budget · Precipitation · wet  
55 enthalpy

56

## 57 **1 Introduction**

58 Equatorial Africa recorded unprecedented amounts of rainfall in October and November 2019  
59 (Wainwright et al, 2020). Such a significant amount of precipitation is not without consequences for  
60 the population and the environment. In October, in most parts of East Africa in general, and in Kenya  
61 in particular, extreme rainfall led to flooding and landslides, provoking major destruction, with more  
62 than 100 deaths and around 18,000 people displaced internally and to neighbouringneighboring  
63 countries (<http://floodlist.com/africa/kenya-floods-november-2019>). In Central Africa, the

64 Democratic Republic of Congo has been devastated by major flooding and forestry disruption along  
65 the Congo River, forcing many people to move (Gou et al. 2022). In the Central African Republic,  
66 extreme and persistent rainfall caused significant flooding and landslides, including the Oubangui  
67 River overflowing nearly 60 km of its coastline (Igri et al. 2023). In addition, the night of 27 to 28  
68 October 2019 was disastrous in the West Cameroon region, mainly in the locality of Bafoussam  
69 where extreme rainfall for about 36 hours caused a landslide, resulting in significant material damage  
70 with 45 dead and others missing (Aretouyap et al. 2021; Mfondoum et al. 2021; Wantim et al. 2023).  
71 The episode was associated with a thermal depression over the Sahara and with anomalously high  
72 Sea Surface Temperatures (SST). The occurrence of these conditions may change in response to  
73 anthropogenic global warming, raising the question of whether devastating events such as the one of  
74 October 2019 could occur more frequently in the future (Nicholson et al. 2022). In particular, given  
75 that climate models predict an increasing trend in extreme rainfall in the region (Fotso-Nguemo et al.  
76 2018, 2019; Sonkoué et al. 2018; Tamoffo et al. 2019, 2023) and that extreme precipitation in the  
77 region is associated with vegetation dynamics (Zhou et al. 2014; Mariotti et al. 2014; Marra et al.  
78 2022; Garcin et al. 2018), it is crucial to understand the thermodynamic and dynamic mechanisms  
79 underlying these exceptional events of October 2019.

80 Recent studies have attempted to investigate the causes of extreme rainfall during the exceptional  
81 period of October 2019 in Equatorial Africa. Nicholson et al. (2022) showed that the heavy rainfall  
82 on the GuineanGuinea coast was reinforcedenhanced by positive sea surface temperature anomalies  
83 along the Atlantic coast. This process leads to On the other hand, a significant advection of the  
84 moisture flux from increase in the flux of moisture originating in the Atlantic, combined with the  
85 convergence of the moisture, which contributed humidity, is another important factor contributing to  
86 the increase in rainfallprecipitation in the region (Pokam et al. 2011, Kuete et al. 2019). Wainwright  
87 et al. (2020) pointed out that the increase in rainfall over East Africa was a consequence of the  
88 positive phase of the Indian Ocean Dipole. Indeed, Black et al. (2005) reported that during periods of  
89 the year when the dipole mode index (DMI) IOD events are greater than 0.5°C over a period of 3  
90 consecutive months and when the zonal SST gradient is reversed over several months, the resulting  
91 increase in rainfall over East Africa is important. In addition, the positive IOD event of 2019 lasted  
92 from late summer through to December, influencing rainfall over East Africa.

93 Rainfall variability in Central Africa is highly dependent on the convergence of atmospheric  
94 moisture (Pokam et al. 2012; Washington et al., 2013; Dyer et al., 2017; Hua et al., 2019; Taguela et  
95 al. 2022). Under the effect of global warming, the increase in extreme precipitation is a consequence  
96 of the increase in available atmospheric humidity (Nicholson et al 2022). Although previous studies  
97 have focused on analyzing meteorological factors, there is still a general lack of knowledge about

98 quantifying the dynamic and thermodynamic effects associated with these extremes of precipitation.  
99 In recent years, the decomposition of the water balance behind precipitation anomalies is often used  
100 to isolate the dynamic and thermodynamic contributions to extreme events (Li et al., 2017; Oueslati  
101 et al., 2019; Wen et al., 2022; Kenfack et al., 2023,2024). Water balance analysis has proved to be a  
102 useful tool for understanding anomaly fields in mean precipitation under the influence of global  
103 warming (Seager et al. 2014). Moist static energy (MSE), in particular, is a useful parameter for  
104 investigating the contribution of atmospheric moisture and analyzing vertical velocity (Wang and Li,  
105 2020a, 2020b; Bell et a. 2015; Neelin, 2021; Nana et al. 2023; Andrews et al. 2023; Longandjo and  
106 Raoul, 2024; Kenfack et al. 2024). Recently, Kenfack et al. (2024) showed that, in the Congo Basin,  
107 the structure of the horizontal moisture advection anomalies is similar to that of the MSE advection  
108 anomalies during rainy seasons March-April-May (MAM) and September-October-November  
109 (SON). In addition, the atmospheric heating source has been identified as an indicator of precipitation  
110 (He et al. 2021). The increase in diabatic heating on the coast can contribute to the acceleration of  
111 near-surface winds (Pokam et al. 2014). An increase in this quantity implies an increase in latent  
112 warming, associated with a strong ocean-continent horizontal moisture gradient, -which can lead to a  
113 strengthening of the boundary layer MSE~~induce the greenhouse effect and reinforce the moisture-~~  
114 convergence, with a positive feedback process leading that leads to extreme precipitation. Further, it  
115 has been demonstrated that a simultaneous reduction in the heating source and rainfall has been  
116 observed in reanalyses over recent decades~~in reducing the source of heating in recent decades has~~  
117 also led to a pronounced reduction in rainfall in reanalyses over the Congo Basin (Kenfack et al.  
118 2024). Given the highlighted importance of moisture, MSE and heating sources on rainfall  
119 variability, we adopt in this study an approach based on diabatic heating, water balance and MSE to  
120 diagnose dynamic and thermodynamic processes associated with the October 2019 rainfall extremes  
121 over West Equatorial Africa.

122 The remainder of the paper is structured as follows. A description of the observation and  
123 reanalysis data, and analysis methods is presented in Section 2. Section 3 describes the diabatic  
124 heating source and the performance of the reanalysis in capturing the October 2019 precipitation  
125 extremes. In Section 4, we investigate the dynamic and thermodynamic effects associated with the  
126 moisture balance. The analysis of the dynamic and thermodynamic effects associated with the MSE  
127 budget during the October 2019 rainfall anomaly period over West Central Africa is presented in  
128 Section 5. Section 6 is conclusions and discussions.

129

## 130 **2 Data and methods**

## 131 2.1. Data

132 In this study, datasets from the fifth version of the European Centre for Medium-Range Weather  
133 Forecasts reanalysis, known as ERA5 (Hersbach et al., 2020), are used for the analyses. Johannsen  
134 et al. (2019) established that over equatorial Africa, ERA5 significantly improves over ERA-  
135 Interim (which represents the previous dataset), particularly in the description of the hydrological  
136 cycle. In addition, Cook and Vizy (2021) have shown that ERA5 represents well the spatial  
137 distribution of precipitation and atmospheric dynamic fields compared with previous generations,  
138 particularly over the Congo Basin. With a spatial resolution of  $0.25^\circ \times 0.25^\circ$ , ERA5 is a global  
139 reanalysis dataset available from 1979 to the present, covering 137 pressure levels from the surface  
140 to 0.01 hPa. Monthly variables including horizontal and vertical wind components, geopotential,  
141 evaporation, humidity, heat flux and temperature are used in this study. For all variables, anomalies  
142 are obtained by removing the 30-year mean of the period 1988 to 2017. To assess ERA5's ability to  
143 detect October 2019 precipitation extremes, we used three observational datasets, including rain  
144 gauge products and gauge-adjusted satellite products: the Climate Hazards Group InfraRed  
145 Precipitation with Stations (CHIRPS) gridded dataset, available at a resolution of  $0.05^\circ \times 0.05^\circ$   
146 (Funk et al., 2015); the Global Precipitation Climatology Project (GPCP-v2.2) with a grid spacing  
147 of  $2.5^\circ \times 2.5^\circ$  (Huffman et al., 2009); the Climatic Research Unit (CRU-TS4.03) gridded data at a  
148 resolution of  $0.5^\circ \times 0.5^\circ$  (Harris et al., 2020).

149

## 150 2.2 Methods

### 151 2.2.1 Diabetic heating

152 Apparent diabatic Diabetic heating as proposed by Yanai and Tomita (1998) and Pokam et al.  
153 (2014) is defined as follows:

$$154 \quad Q = \chi \left( \frac{\partial \theta}{\partial t} + u \frac{\partial \theta}{\partial x} + v \frac{\partial \theta}{\partial y} + \omega \frac{\partial \theta}{\partial p} \right) \quad (1)$$

$$155 \quad \chi = c_p \left( \frac{T}{\theta} \right) \quad (2)$$

156 In equations 1 and 2,  $C_p$  ( $1,005 \text{ J Kg}^{-1} \text{ K}^{-1}$ ) denotes the specific heat at constant pressure,  $\theta$  is the  
157 potential temperature,  $\omega$  is the vertical velocity ( $\text{hPa s}^{-1}$ ), and  $V$  and  $V$   $= (u, v)$  is the vector of  
158 horizontal velocities.  $T$  (K) and  $p$  (hPa) represent the air temperature and the barometric pressure,  
159 respectively.

160 To quantify the monthly mean heating rate  $\tau$  ( $\text{K day}^{-1}$ ) related to apparent heating, we use the  
161 relation:

$$\tau = \frac{Q}{c_p} \quad (3)$$

162 where  $Q$  is the combination of heat from radiation, latent heat from condensation and the  
163 convergence of vertical vortical transport of sensible heat.

164

### 165 2.2.2 Diagnosis of the moisture budget

166 The moisture budget used to quantify the contributions of evaporation and the horizontal and  
167 vertical components associated with the circulation of moist air in the atmosphere (Seager et al.,  
168 2010; Oueslati et al., 2019; Jiang et al., 2020; Moon and Ha, 2020; Wen et al., 2022; Zhao et al.,  
169 2022; Sheng et al., 2023; Kenfack et al., 2024) is defined as follows:

$$170 \langle \partial_t q \rangle + \langle \mathbf{V} \cdot \nabla_h q \rangle + \langle \omega \cdot \partial_p q \rangle = E - P \quad (4)$$

171 In Eq. 4,  $q$  represents the specific humidity,  $\mathbf{V}=(u,v)$  denotes the horizontal wind and  $\omega$  the vertical  
172 pressure velocity.  $E$  denotes surface evaporation and  $P$  precipitation. Angle brackets " $\langle \rangle$ "  
173 signify the mass integral from the surface ( $p_s = 1000$  hPa) to a pressure  $p_t = 300$  hPa,  
174 which -which, as specified by Seager et al. (2010), represents the top of the atmosphere layer  
175 considered. The first term on the left of equation 4 can be neglected given its small variation because  
176  $q$  varies little over time on a monthly scale and could contribute to the residuals. To estimate the  
177 horizontal and vertical moisture advection components, we decompose equation 4 into its different  
178 linear and residual terms as follows:

$$179 P' = E' - \langle \mathbf{V}' \cdot \nabla q' \rangle - \langle \mathbf{V}' \cdot \nabla \bar{q} \rangle - \langle \bar{\omega} \partial_p q' \rangle - \langle \omega' \partial_p \bar{q} \rangle + Res \quad (5)$$

180 In Eq. 5, the overbar indicates the monthly mean climatology from 1988 to 2017 and primes  
181 indicate deviations from this climatology; The residual term "Res" contains the non-linear and  
182 transient processes associated with the joint variations in water vapor content and circulation. The  
183 terms  $\langle -\mathbf{V}' \cdot \nabla \bar{q} \rangle$  and  $\langle -\omega' \partial_p \bar{q} \rangle$  represent the dynamic contributions (or effect) and refer to  
184 the moisture advection induced by the horizontal wind and by the vertical pressure velocity,  
185 respectively. The terms  $\langle -\mathbf{V}' \cdot \nabla q' \rangle$  and  $\langle -\bar{\omega} \partial_p q' \rangle$  represent the thermodynamic contributions  
186 (or effect), and refer to the contribution of water vapor.

187

### 188 2.2.3 Diagnosis of the MSE budget

189 The MSE equation is defined as follows:

$$190 \langle \partial_t (c_v T + L_v T) \rangle + \langle \mathbf{V} \cdot \nabla M \rangle + \langle \omega \partial_p m \rangle = F_{net} \quad (6)$$

191 where the moist enthalpy is

193 
$$M = c_p T + L_v q \quad (7)$$

194 and the MSE is

195 
$$m = c_p T + L_v q + \Psi \quad (8)$$

196 In equations 7 and 8,  $c_p$  ( $c_v$ ) ~~represents~~ represent the specific heat at constant pressure ( the specific  
 197 heat at constant volume); T is the air temperature and  $\Psi$  the geopotential.  $F_{net}$  is the net energy  
 198 entering the atmospheric column at the surface and top of the atmosphere (latent heat, sum of  
 199 sensible heat, and shortwave and longwave radiative fluxes). Similar to the moisture flux equation,  
 200 the first term on the left of equation 6 can be neglected given its small variation over time on a  
 201 monthly scale and contributes to the residuals. In addition, it should be noted that variations in  
 202 geopotential height along pressure levels are neglected in this formulation of the MSE budget. The  
 203 remaining terms in. The remainder of equation 6 can be decomposed into horizontal and vertical  
 204 advection components, as described by:

205 
$$\langle \omega' \partial_p \bar{m} \rangle = -\langle \nabla \cdot \nabla M' \rangle - \langle V' \cdot \nabla M \rangle - \langle \omega \partial_p m' \rangle + F'_{net} + Res \quad (9)$$

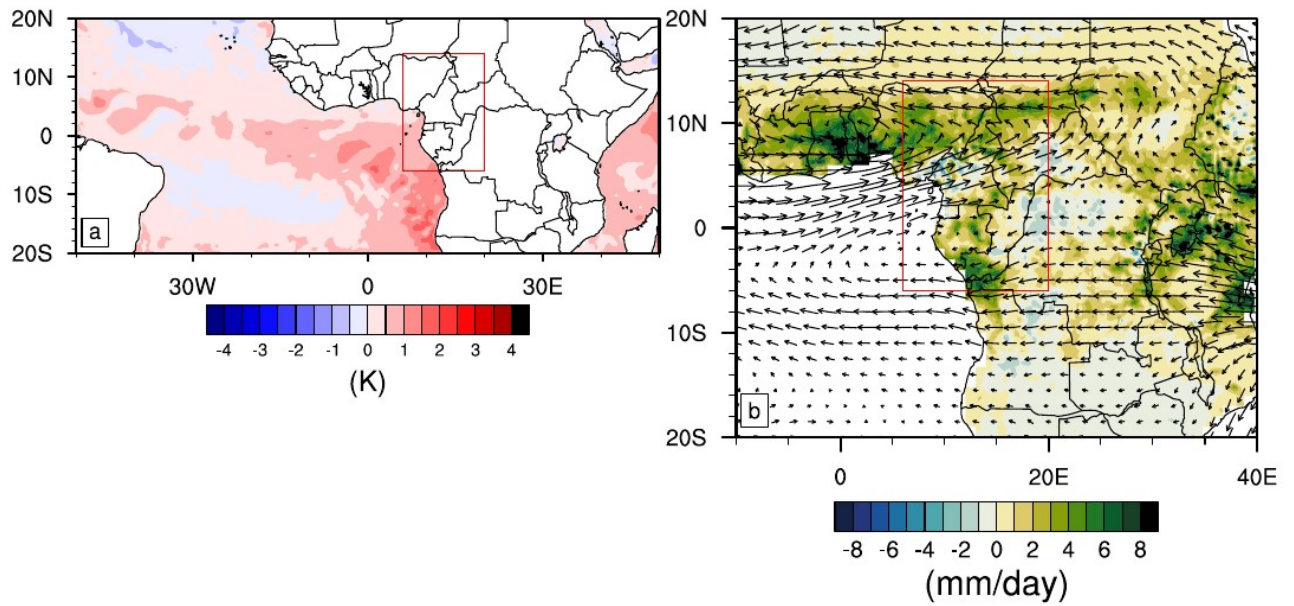
206 Anomalous vertical motion is ~~analysed~~ analyzed using this equation with a given profile of  $\bar{m}$ .  
 207 Similar to the convention adopted for decomposing the moisture flux, the term  $-\langle V' \cdot \nabla M \rangle$   
 208 relates to the anomalous MSE associated with the atmospheric circulation and contains the dynamic  
 209 contribution (or effect), while the two terms  $-\langle \nabla \cdot \nabla M' \rangle$  and  $-\langle \omega \partial_p m' \rangle$  refer to the  
 210 thermodynamic contribution (or effect), which is crucial for diagnosing the thermal state of the  
 211 atmosphere associated with the increase in the vertical rise of the air.

### 212 3 Diabatic heating and extreme rainfall

213 ~~The As mentioned earlier, the~~ increase in SSTs in the eastern Atlantic (Fig. 1a) ~~is has been~~  
 214 identified as one of the causes of the positive precipitation anomalies over western central Africa  
 215 inin West Central Africa during October 2019. ~~(Nicholson et al. 2022).~~ The warming contrast  
 216 between the ocean and the continent favoured the strengthening of the moisture advection  
 217 associated with the precipitation anomalies over West Central Africa (Fig. 1b). This is in agreement  
 218 with Nicholson can lead to significant diabatic heating over the continent, thereby favoring  
 219 atmospheric instability (Pokam et al. (2022), 2014).

220 ~~— Figure 1 represents the mean vertical profile (pressure-latitude) of diabatic heating averaged~~  
 221 ~~between 6° and 20°E during SON for the 1988-2017 climatology (Fig. 1a) and the corresponding~~

222 | profile for 2019 (Fig. 1b). During SON, the main source of heat is located between 3°S and 9°N for  
223 | climatology, and between 5°S and 13°N for 2019.

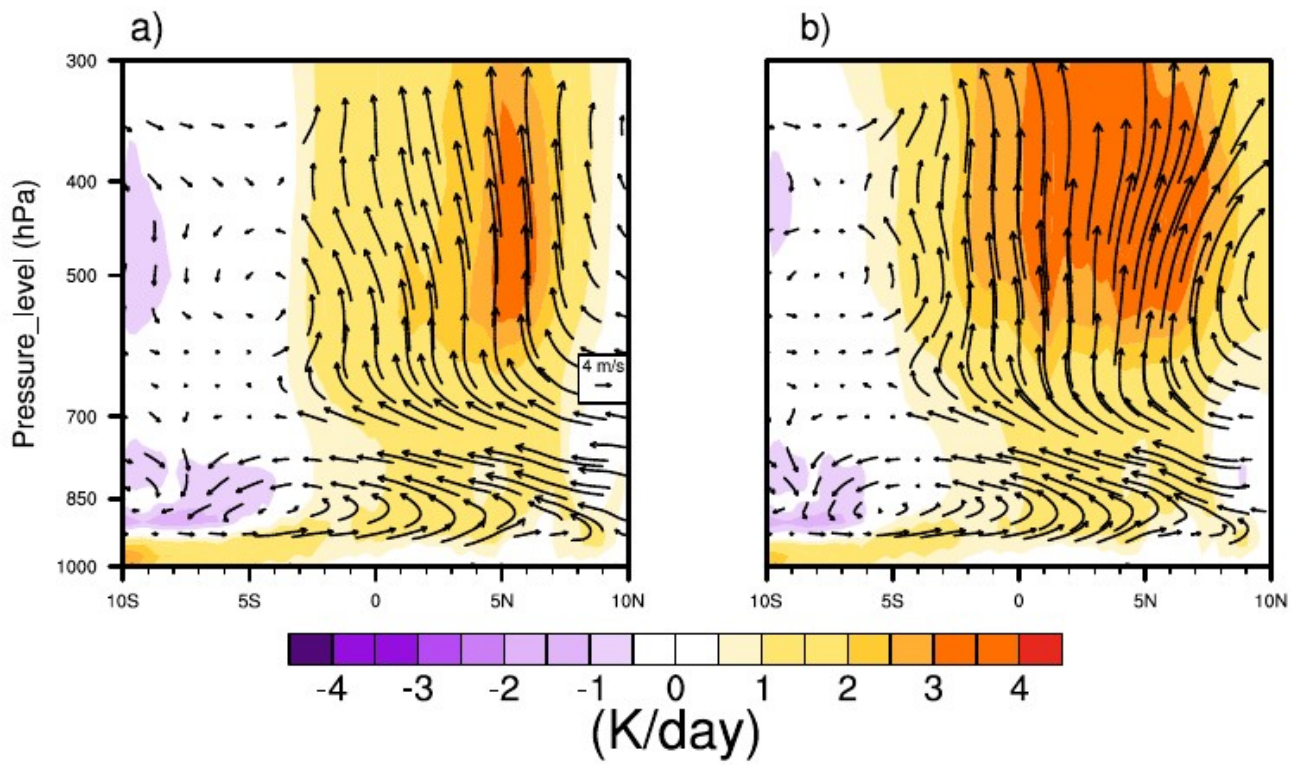


224

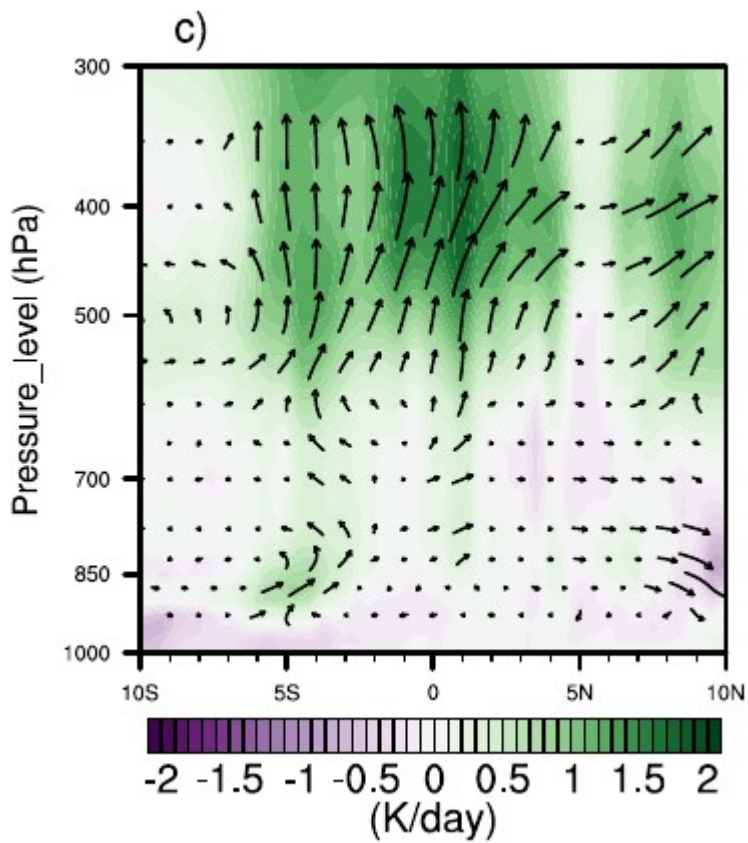
225 | **Fig 1.** SST a) and rainfall b) anomalies during October 2019. The vectors represent anomalies of  
226 | vertically integrated atmospheric moisture flux. The red box indicates the Central West Africa area.

227 | Figure 2 represents the mean vertical profile (pressure-latitude) of diabatic heating averaged  
228 | between 6° and 20°E during SON for the 1988-2017 climatology (Fig. 2a) and the corresponding  
229 | profile for 2019 (Fig. 2b). During SON, the main source of heat is located between 3°S and 9°N for  
230 | climatology, and between 5°S and 13°N for 2019.





231



232

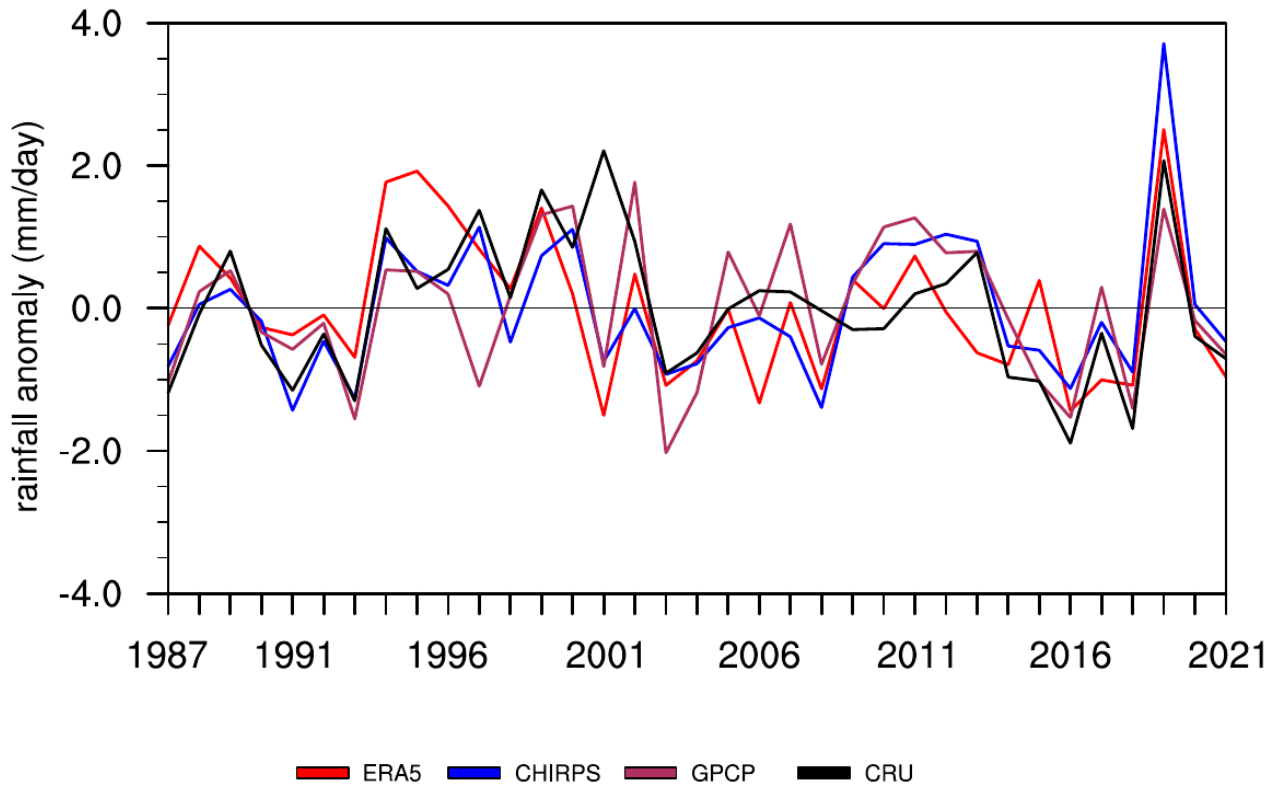
233 **Fig 21.** Diabatic heating and divergent meridional circulation (vectors;  $m s^{-1}$ ) during the SON  
 234 season for a) the 1988-2017 avg, b) 2019 avg and c) climatology and b) the anomaly 2019-mean, all

235 averaged between the 6° and 20°E. As the vertical velocity is much weaker than the meridional  
236 wind, its values have been enhanced by a factor of 600 for the clarity of the graph.

237

238 However, 2019 presents a more extensive and pronounced source of heat compared with the  
239 climatology 1988-2017. A 3-4  $K day^{-1}$  heating, more intense in 2019, occurred from 600 hPa. A  
240 cooling of 1- 2  $K day^{-1}$  took place around 850 hPa in the south and from 550 hPa in the north. The  
241 profound heating observed from 600 hPa originates at the surface on the southern portion of the  
242 domain (10°S). It is reinforced by the contrast between the large positive values and the negative  
243 values on either side of the equator between 500 and 400 hPa. The vertical structure of the  
244 divergent circulation is also illustrated in Figure 21. The divergent circulation appears more  
245 pronounced from 550 hPa in 2019 (Fig. 2b4b) compared with the climatology of 1988-2017 (Fig.  
246 2a4a). This is consistent with the warming contrast observed. This uplift was reinforced by the  
247 warming of the equatorial Atlantic associated with an abnormally strong thermal low over the  
248 Sahara, which led to an acceleration of the dominant meridional flow in the divergent circulation.  
249 (Fig. 2c). This is in agreement with Nicholson et al. (2022), who highlighted that the West African  
250 monsoon was late to withdraw in 2019.

251 Although the SON season has shown significant diabatic heating compared to climatology,  
252 October 2019 in particular over West Central Africa recorded extremes of rainfall (Nicholson et al.  
253 2022). In this study, we use the ERA5 reanalysis precipitation fields for water balance analysis.  
254 This ensures that all the examined physical quantities are consistent across the study. Before doing  
255 so, we assessed the performance of ERA5 in detecting the extreme precipitation events in October  
256 2019. Figure 32 illustrates the interannual variability of October rainfall anomalies over West  
257 Central Africa for the period 1987-2021.



258

259 **Fig 32.** Temporal evolution of October rainfall anomaly over West Central Africa ([6°S-14°N, 6°-](#)  
 260 [20°E](#)), from reanalysis data ERA5, from the ERA5 reanalysis dataset (red) and from observational  
 261 data CHIRPS (blue), GPCP (maroon) and CRU (black), covering the period 1987–2021.

262

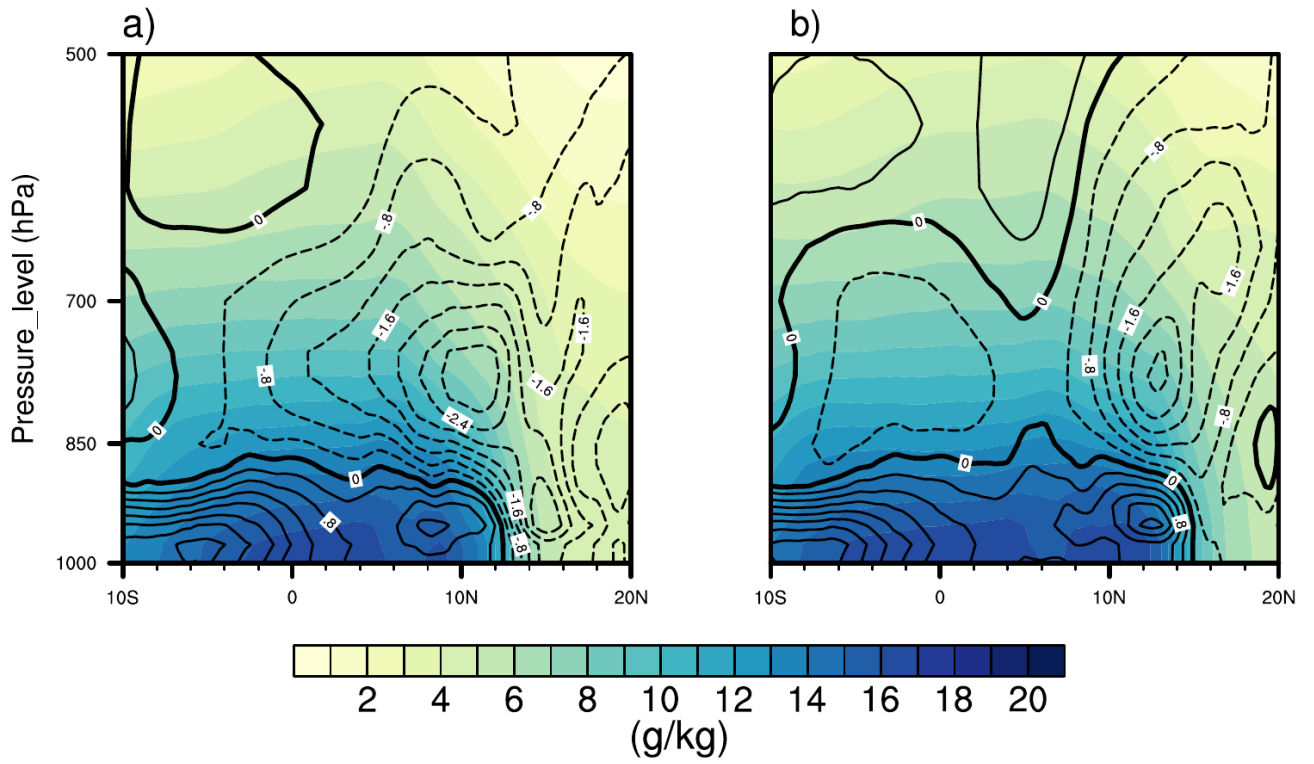
263 The ERA5 reanalysis (red) and the CHIRPS (blue), GPCP (maroon) and CRU (black) observations  
 264 are consistent in highlighting the high precipitation peak of 2019. CHIRPS shows the highest values  
 265 of positive anomalies of up to 3.5 mm day<sup>-1</sup>, while ERA5 shows values of up to 2.5 mm day<sup>-1</sup>.

266 Despite some differences between ERA5 and the observations in representing trends on an  
 267 interannual scale (Kenfack et al. 2024), the unprecedented event of October 2019 was well detected.

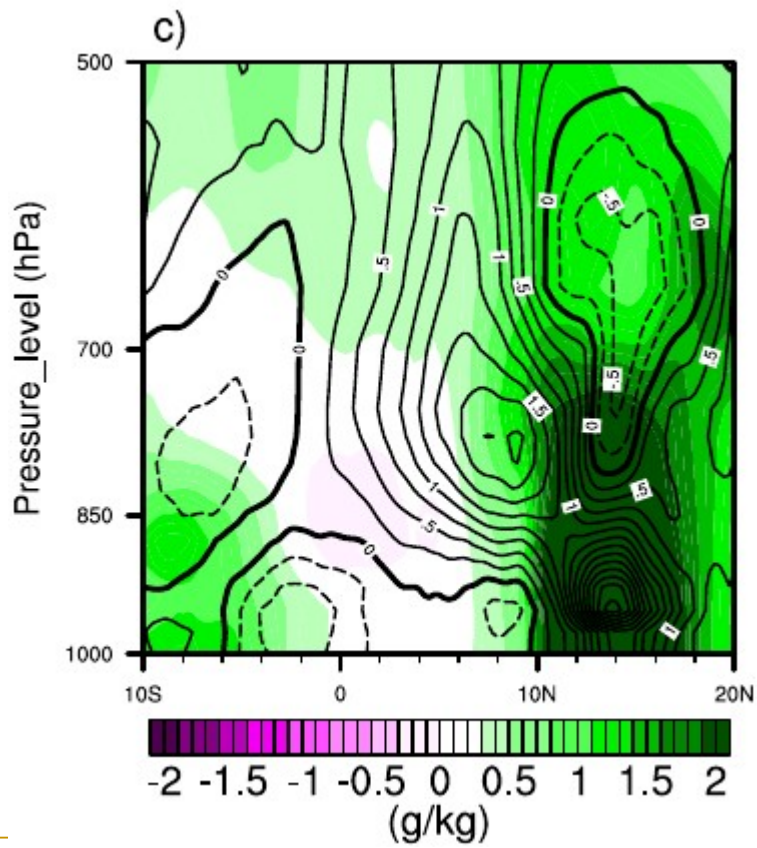
268 [In addition, the exceptional event is also detected by the MERRA2 reanalysis \(Figure S1\)](#)

269 The increase in SSTs in the [tropicalequatorial](#) Atlantic reached a record level [induring](#) October  
 270 2019 [\(Nicholson et al. 2022\)](#). This may have resulted in an increased specific humidity over land.

271 Figure [43](#) depicts the vertical profile (pressure level-latitude) of specific humidity (colors) and  
 272 meridional wind (contours) averaged between 6° and 20°E for the 1988-2017 climatology (Fig.  
 273 [4a3a](#)), the October 2019 average (Fig. [4b3b](#)), and the October 2019 anomaly (Fig. [4c3c](#)).



274



275

276 **Fig. 43.** Specific humidity and meridional wind (contours: m/s) in October for a) [1988-2017 avg](#) the  
 277 [climatology of 1988-2017](#), b) 2019 [avg](#) and c) the anomaly, averaged between 6°-20°E.

278

279

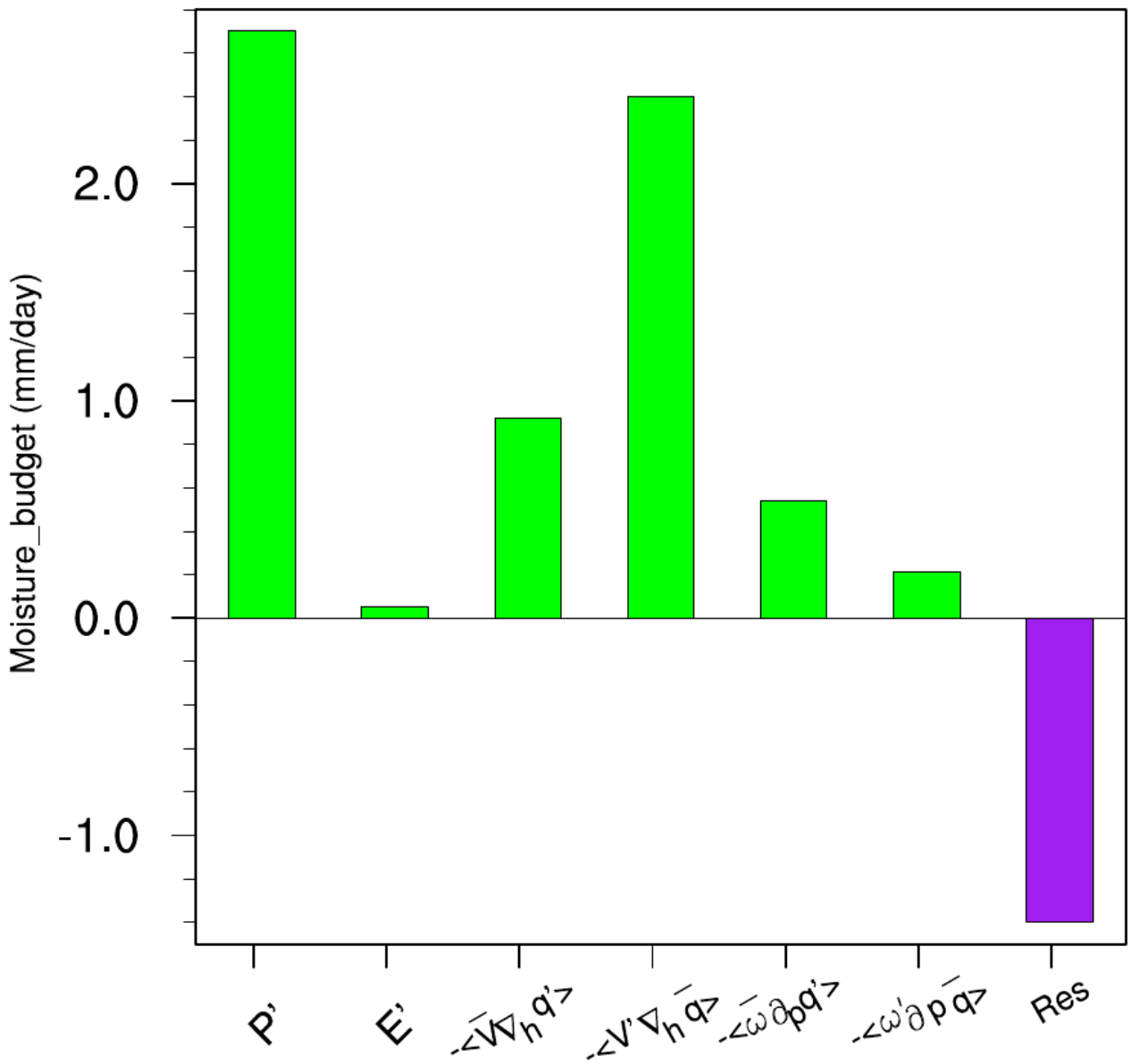
280 The 1988-2017 climatology is characterized by intense surface specific humidity extending as far as  
281 12°N, whereas the October 2019 average appears to extend further to 15°N. In addition, the  
282 southerly wind in 2019 was more pronounced up to 15°N compared to the climatology. Analysis of  
283 the anomalies ~~Anomaly analysis~~ confirms that the humidity extended further north in West  
284 Central ~~there was more moisture in equatorial central~~ Africa in October 2019, compared with-  
285 compared to the climatology. The intensification of the southerly wind up to 15°N indicates that  
286 this moisture probably comes from the equatorial Atlantic. This is in agreement with Kamae et. al  
287 (2017), who highlighted that extreme precipitation can be a consequence of changes in humidity.  
288 Indeed, the increase in humidity associated with a substantial heating source contributes to an  
289 increase in precipitation. In addition, In the case of the monthly anomalies, the changes in the winds  
290 are thought to ~~Chadwick et al. (2016) showed that increased humidity over land would~~ be a  
291 response to the increased moisture advection from the oceans as a result of global ~~under~~ warming.

#### 292 **4 Moisture budget analysis**

293 Rainfall variability in equatorial Central Africa is strongly dependent on the moisture inputs  
294 associated with atmospheric circulation (Jackson et al., 2009; Cook and Vizy, 2016, 2022; Dyer et  
295 al., 2017; Longandjo and Raoul, 2024). In the Congo Basin, atmospheric heating sources combined  
296 with the vertical advection of moisture induced by anomalous vertical motion are responsible for  
297 most of the interannual variability of precipitation (Kenfack et al., 2024). In this section, we  
298 decompose the moisture budget in equation 5 to examine the processes that led to the October 2019  
299 extreme rainfall over West Central Africa. To do this, we analyse ~~analyze~~ local variations in rainfall  
300 associated with atmospheric moisture introduced into the air column by atmospheric circulation.

301 The monthly anomalies of the different components of the water balance averaged over the  
302 northern part of west-central Africa (6°N-14°N, 6°-20°E) for the month of October 2019 (Fig. 5)  
303 indicate that the increase in dynamic processes dominated the increase in precipitation. Horizontal  
304 advection of moisture induced by the horizontal wind anomaly  $\langle -\mathbf{V}' \cdot \nabla \bar{q} \rangle$  was the most  
305 pronounced component (up to 2.5 mm/day). Although thermodynamic processes  $\langle -\nabla \cdot \nabla q' \rangle$  and  
306  $\langle -\bar{\omega} \partial_p q' \rangle$  are weaker than dynamic processes, they also contributed to the extreme rainfall  
307 amounts. Evaporation  $E$ , for its part, contributed very little (0.1 mm/day). This is consistent with  
308 Cook et al. (2019) who found that rainfall anomalies in equatorial Central Africa do not depend

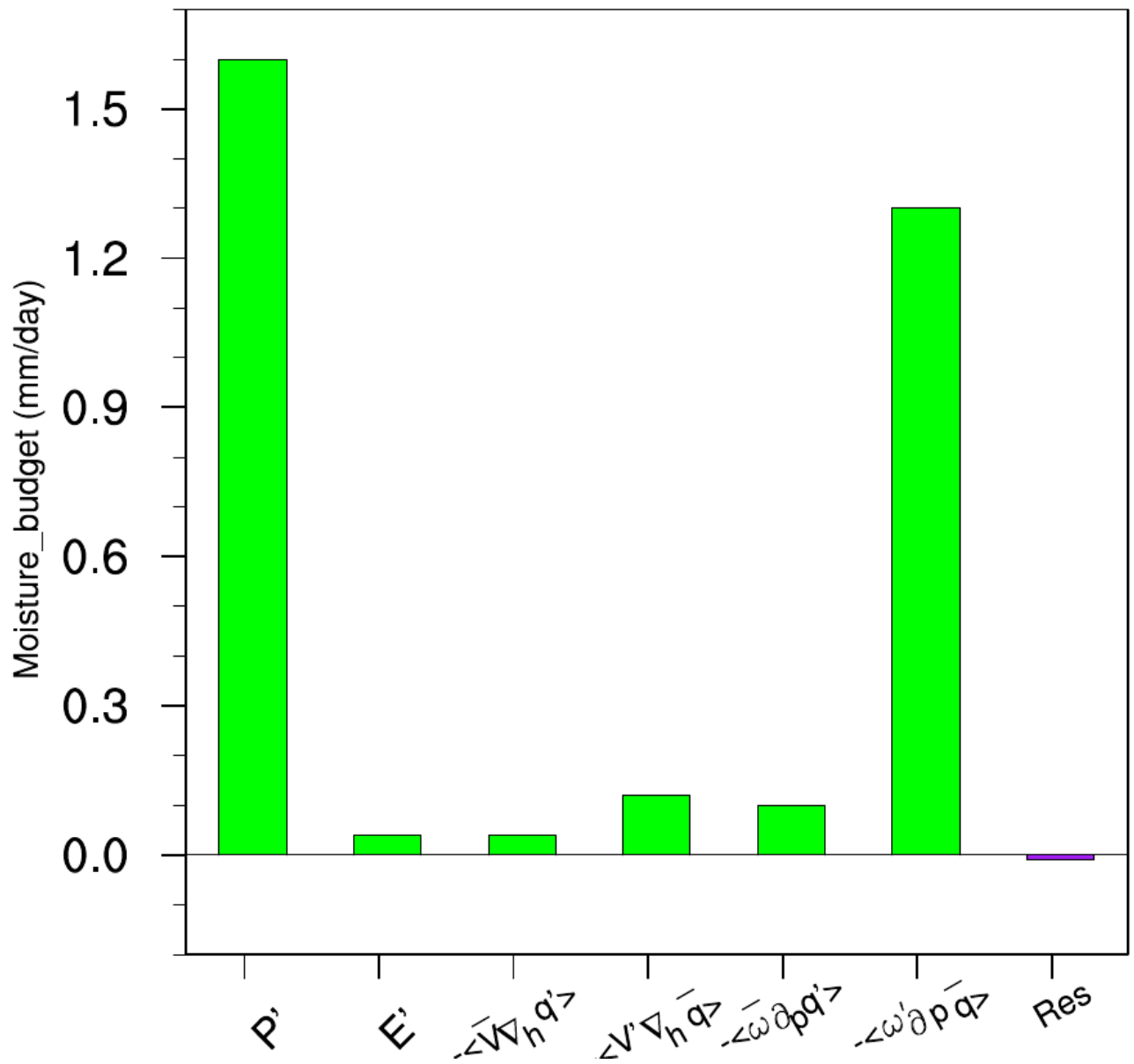
309 directly on surface heating. It should also be noted that the residual term for a value of -1.2 mm/day  
310 is considerable. Indeed, the northward shift and strengthening of the northern component of the  
311 East African Jet (AEJ-N) in October are verified (Nicholson et al. 2022). This is illustrated by the  
312 anomalous 700 hPa zonal wind in October 2019. In addition, the anomalous variance of the band-  
313 pass filtered 700 hPa meridional wind over 2-6 days is also visible, indicating African easterly wave  
314 activity (Reed et al., 1977). Other studies also point out that rainfall fluctuations in equatorial  
315 Africa are associated with Kelvin waves (Jackson et al., 2019). The residual term could influence the  
316 estimation of dynamic and thermodynamic distributions in the water budget. Analysis of the  
317 components of the water balance over the western part of the Congo Basin (6°S-5°N, 6°-20°E) for  
318 October 2019 (Fig. 6) shows that the increase in rainfall was dominated by vertical advection of  
319 moisture induced by changes in vertical velocity  $\langle -\omega' \partial_p \bar{q} \rangle$  (1.4 mm/day ). However, the  
320 contributions of the other processes, including the residual term, are low.



321

322 **Fig. 5** Monthly mean anomalies in moisture budget for October 2019, averaged over the Northern  
 323 part of West Central Africa (6°N-14°N, 6°-20°E).

324 — The monthly anomalies of the different components of the water balance averaged over West  
 325 Central Africa (6°S-14°N, 6°-20°E) for October 2019 (Fig. 4) indicate that the increase in rainfall  
 326 was dominated by the increase in dynamic processes.

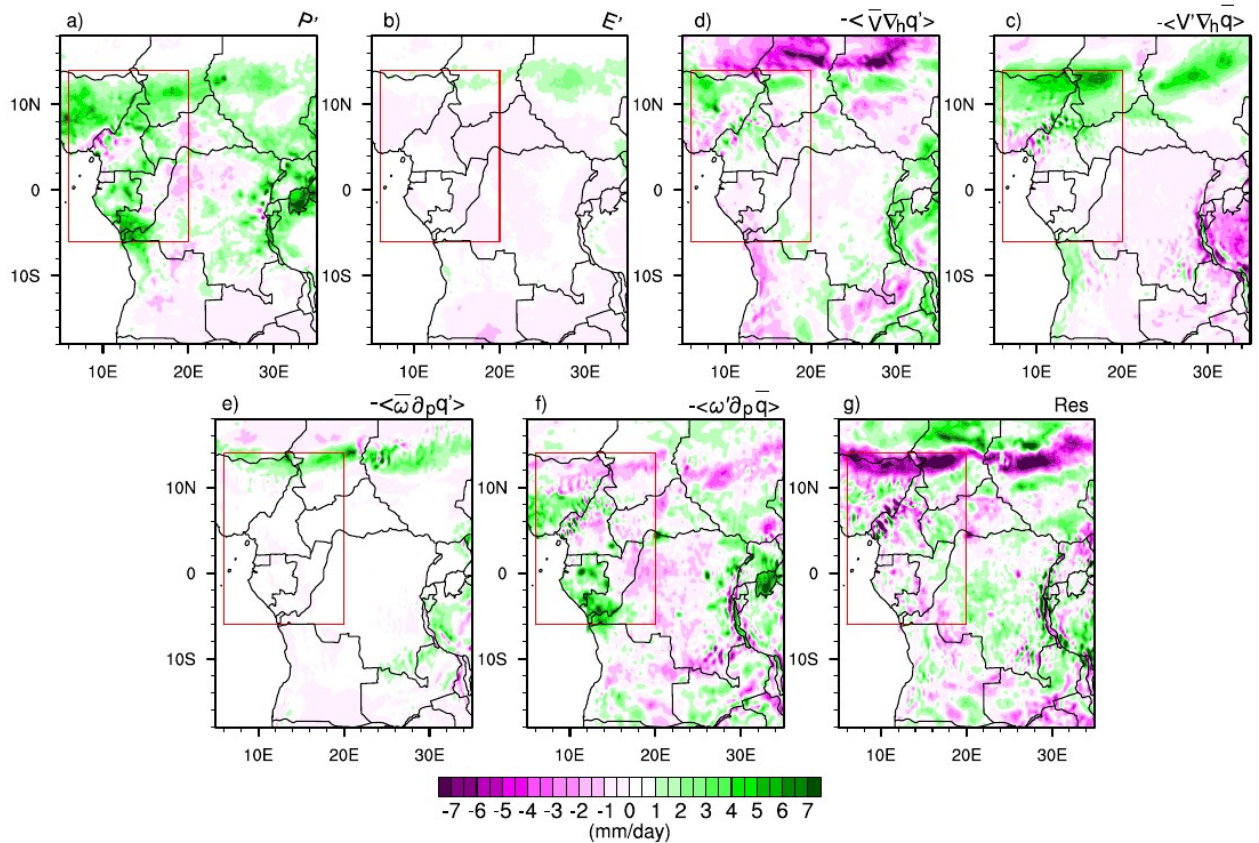


327

328 **Fig. 6.** Monthly mean anomalies in moisture budget for October 2019, averaged over the Southern  
 329 part of West Central Africa (6°S-5°N, 6°-20°E).

330 At the pixel scale, positive precipitation anomalies over eastern Nigeria, southern Chad and  
 331 northern Cameroon (Fig. 7a) were mainly dominated by horizontal moisture advection induced by  
 332 the horizontal wind anomaly (Fig. 7d). Over Gabon, south of Congo Brazzaville, positive  
 333 precipitation anomalies were dominated by vertical moisture advection induced by vertical  
 334 anomalous motion (Fig. 7f). Horizontal moisture advection induced by the specific humidity  
 335 anomaly (Fig. 7c), although not the key factor associated with precipitation patterns, shows a small  
 336 positive contribution over the northern part of the domain.





337

338 **Fig. 7.** Spatial distributions of each term of the water budget equation during October 2019 over West  
 339 Equatorial Africa (Red box). (a) Precipitation anomalies, (b) evaporation anomaly, (c) horizontal  
 340 advection of anomalous moisture by climatological wind, (d) horizontal advection of climatological  
 341 moisture by anomalous wind, (e) vertical advection of anomalous moisture by climatological vertical  
 342 velocity, (f) vertical advection of climatological moisture by anomalous vertical velocity and (g) the  
 343 residual term.

344 **Fig. 4.** Monthly mean anomalies in moisture budget for October 2019, averaged over West  
 345 Equatorial Africa ( $6^{\circ}\text{S}$ - $14^{\circ}\text{N}$ ,  $6^{\circ}$ - $20^{\circ}\text{E}$ ) as indicated by the red box in Fig. 2a.

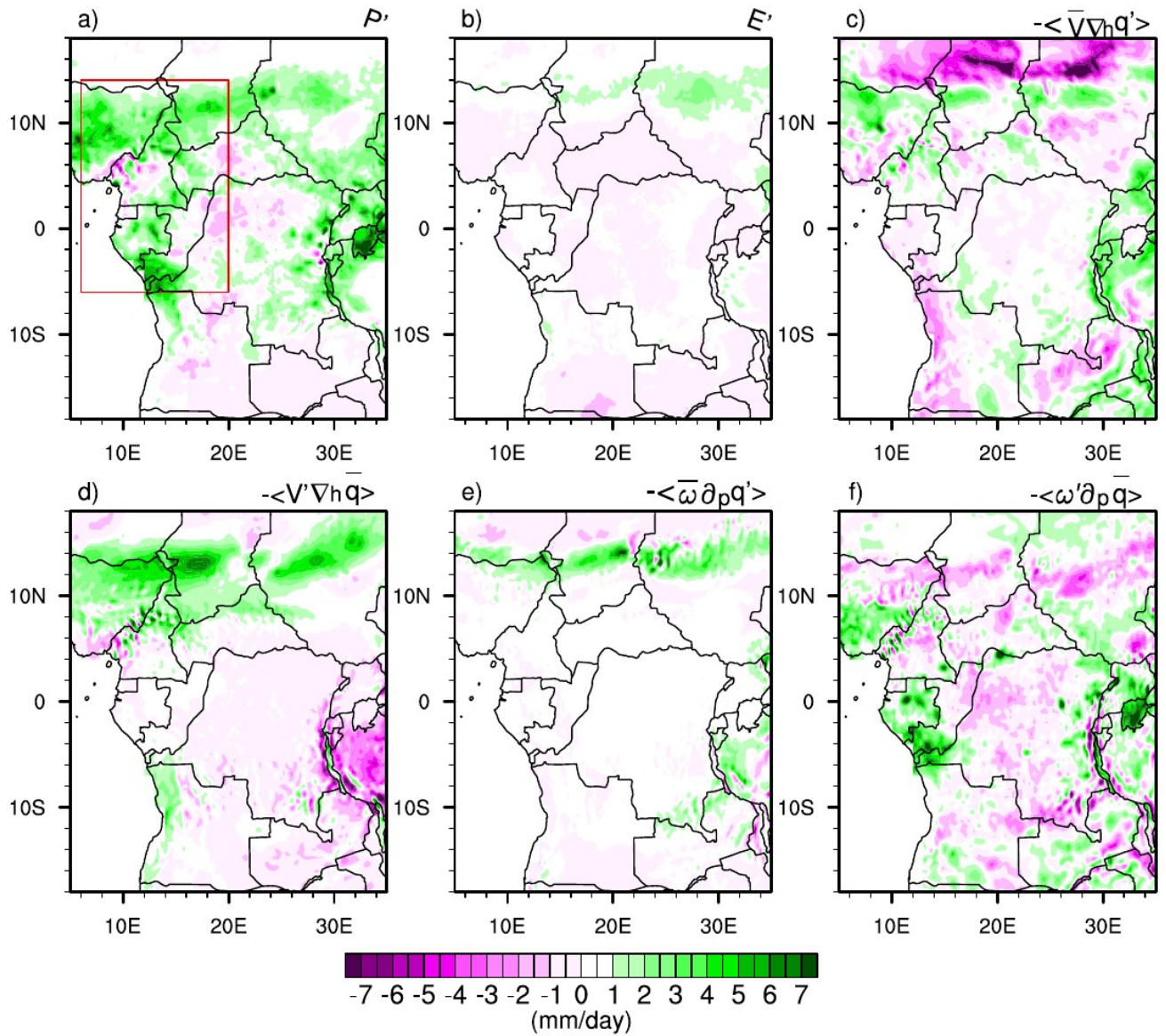
346

347 The contribution of evaporation (Fig. 7b) and horizontal advection of moisture induced by the  
 348 specific humidity anomaly (Fig. 7e) remains weak over the entire domain, although some positive  
 349 values can be seen around  $14^{\circ}\text{N}$ . This result is similar to that provided by MERRA2 (Figure S2).  
 350 Thermodynamic effects reflect the change in the thermal state of the atmosphere associated with the  
 351 October 2019 rainfall extremes over West Central Africa. It should be noted that changes in the  
 352 thermal state of the atmosphere may allow us to speculate on the potential role of global warming in  
 353 rainfall variations in 2019, even without considering potential impacts on atmospheric dynamics.

354 However, changes in the thermodynamic effect, although not the key factor responsible for the  
355 October 2019 events, contributed up to 35% of the total effect (the sum of dynamic and  
356 thermodynamic contributions) on the northern part and 15% on the southern part of the domain.  
357 This could be since the increase in diabatic heating contributes to the change in the thermal state  
358 of the atmosphere, i.e. the increase in thermodynamic effects (changes in humidity). In fact,  
359 Nicholson et al. (2022) reported that the increase in SST in the tropical Atlantic strengthened the  
360 advection of moist air from the Atlantic towards the region, with an increase in the moisture flux  
361 from the west to southwest.

362 ~~Horizontal advection of moisture induced by the horizontal wind anomaly  $\langle -\mathbf{v}' \cdot \nabla \bar{q} \rangle$  was the~~  
363 ~~most pronounced component (up to 1.2 mm/day), followed by the vertical advection of moisture~~  
364 ~~induced by the vertical velocity anomaly  $\langle -\omega' \partial_p \bar{q} \rangle$  (1 mm/day). Although thermodynamic~~  
365 ~~processes  $\langle -\nabla \cdot \nabla q' \rangle$  and  $\langle -\bar{\omega} \partial_p q' \rangle$  are weaker than dynamic processes, they also contributed~~  
366 ~~to the extreme rainfall amounts. Evaporation  $E$ , for its part, contributed very little (0.1 mm/day).~~  
367 ~~This is consistent with Cook et al. (2019) who found that rainfall anomalies in equatorial Central~~  
368 ~~Africa do not depend directly on surface heating. It should also be noted that the residual term for a~~  
369 ~~value of -1.1 mm/day is considerable. This could be due to the fact that the Madden-Julian~~  
370 ~~Oscillation (MJO) was active over Africa, particularly in October (Wainwright et al, 2020), which~~  
371 ~~probably developed nonlinear oscillatory weather systems.~~

372 ~~— At the pixel scale, positive precipitation anomalies over eastern Nigeria, southern Chad and~~  
373 ~~northern Cameroon (Fig. 5a) were mainly dominated by horizontal moisture advection induced by~~  
374 ~~the horizontal wind anomaly (Fig. 5d). Over Gabon, south of Congo Brazzaville, positive~~  
375 ~~precipitation anomalies were dominated by vertical moisture advection induced by vertical~~  
376 ~~anomalous motion (Fig. 5f). Horizontal moisture advection induced by the specific humidity~~  
377 ~~anomaly (Fig. 5c), although not the key factor associated with precipitation patterns, shows a small~~  
378 ~~positive contribution over the northern part of the domain.~~



379

380 **Fig. 5.** Spatial distributions of each term of the water budget equation during October 2019 over West-  
 381 Equatorial Africa. (a) Precipitation anomalies, (b) evaporation anomaly, (c) horizontal advection of  
 382 anomalous moisture by climatological wind, (d) horizontal advection of climatological moisture by  
 383 anomalous wind, (e) vertical advection of anomalous moisture by climatological vertical velocity and (f)  
 384 vertical advection of climatological moisture by anomalous vertical velocity.

385

386 The contribution of evaporation (Fig. 5b) and horizontal advection of moisture induced by the  
 387 specific humidity anomaly (Fig. 5e) remains weak over the entire domain, although some positive  
 388 values can be seen around 14°N. Thermodynamic effects reflect the change in the thermal state of  
 389 the atmosphere associated with the October 2019 rainfall extremes over West Central Africa. It  
 390 should be noted that changes in the thermal state of the atmosphere may allow us to speculate on

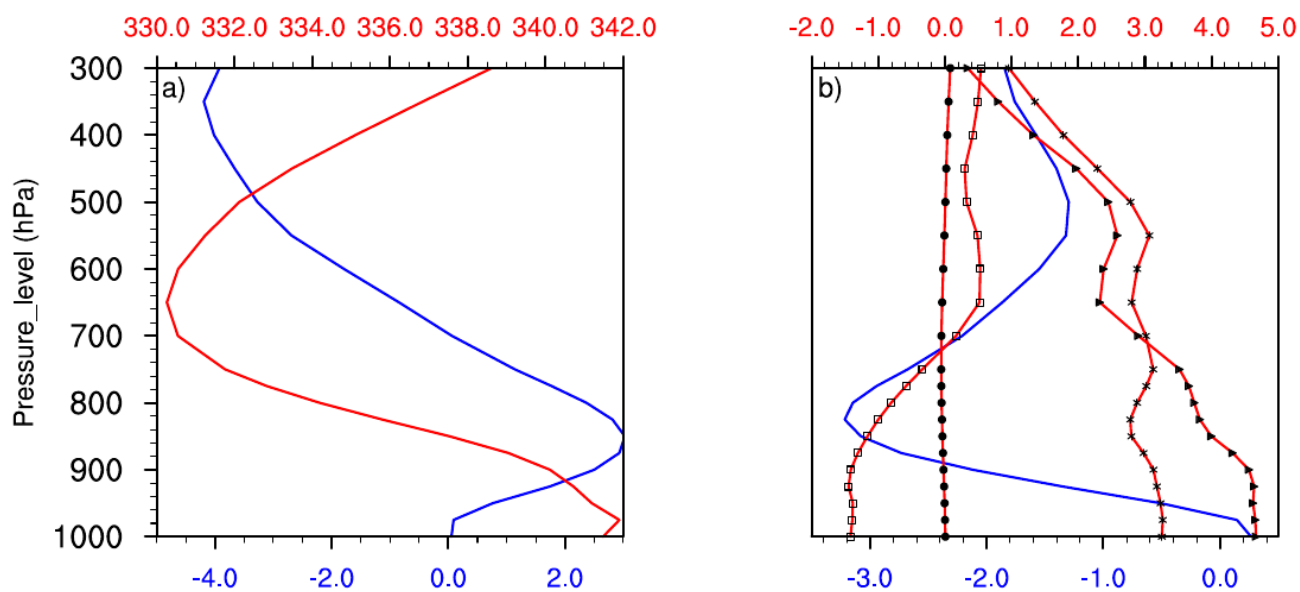
391 the potential role of global warming in rainfall variations in 2019, even without considering  
392 potential impacts on atmospheric dynamics. However, changes in the thermodynamic effect,  
393 although not the key factor responsible for the October 2019 events, contributed up to 27.5% of the  
394 total effect (the sum of dynamic and thermodynamic contributions). This could be due to the  
395 increase in atmospheric humidity on the one hand and the increase in diabatic heating on the other.  
396 The increase in atmospheric humidity could be related to the increase in SSTs in the equatorial  
397 Atlantic at the same time of year as highlighted by Nicholson et al. (2022).

## 398 5 MSE budget analysis

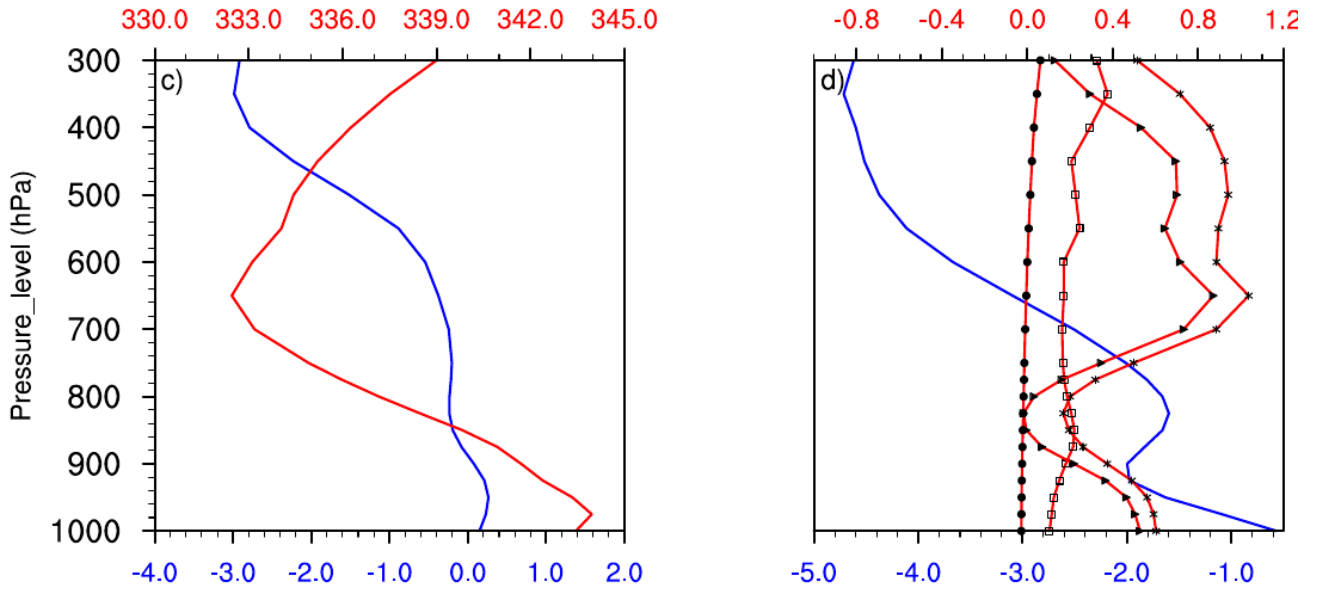
399 The previous results clearly showed that the vertical advection of moisture induced by the  
400 vertical velocity anomaly was identified as the second dynamic parameter (after the horizontal  
401 advection of moisture induced by the anomalous horizontal movement) contributing to the  
402 increase in precipitation in October 2019. Diagnosis contributing to the increase in precipitation in  
403 October 2019. To better understand the creation and maintenance of the structure of vertical  
404 motion, we can base ourselves on the diagnosis of the MSE budget, which takes account of into  
405 account the thermal state of the atmosphere and as well as the effect of atmospheric circulation, is  
406 used to analyse the atmospheric perturbation related to moisture transport. The MSE largely  
407 influences the structure of vertical motion. The structure of vertical motion is largely influenced by  
408 the MSE. In addition, diagnosis of the MSE balance emphasises emphasizes the relative  
409 contributions of temperature, specific humidity and atmospheric circulation associated with the  
410 vertical motion anomaly.

411 The vertical profiles of the vertical velocity anomaly  $\omega'$  and the MSE climatology  $\bar{m}$   
412 averaged over the north of the domain are shown in Figure 8a. The vertical velocity anomaly  $\omega'$   
413 shows positive values at the surface and negative values in the middle and upper troposphere. The  
414 alternation of positive and negative values in the tropospheric column probably reduces the  
415 contribution of the vertical advection of moisture induced by the anomalous vertical motion. The  
416 MSE climatology  $\bar{m}$  exhibits a bottom-heavy bove structure with a minimum around 650 hPa.  
417 Such a structure generally indicates that  $\langle \partial_p \bar{m} \rangle < 0$  (Chen and Bordoni, 2014; Liu et al. 2021; Wen  
418 et al. 2022). As a result, positive (negative) values of  $\langle \omega' \partial_p \bar{m} \rangle$  depends on the vertical structure of  
419 the omega anomalies. The vertical velocity climatology  $\bar{\omega}$  (Fig. 8b) is negative over the entire  
420 troposphere, characterising an upward movement. The MSE anomaly  $m'$  decreased slightly near  
421 the surface then increased from 800 hPa to 550 hPa, with a minimum value around 550 hPa.

422 However, this includes three terms, namely,  $gz'$  which is weak in the entire tropospheric column,  
 423 the enthalpy anomaly  $c_p T'$ , which tends to increase, and  $l_v q'$ , tends to behave similarly to  $m'$   
 424 between 650 hPa and 300 hPa. To the south of the domain (Fig. 8c), the vertical velocity anomaly  
 425 shows negative



426  
 427 ——— The vertical profiles of the vertical velocity anomaly  $\omega'$  and the MSE climatology  $\bar{m}$  are  
 428 shown in Figure 6a.



429

430 **Fig. 86.** Vertical profile of a) vertical velocity anomaly  $\omega'$  (bluegreen line:  $10^{-2} Pa.s^{-1}$ ) and  
 431 MSE climatology  $\bar{m}$  (red line:  $10^3 J.Kq^{-1}$ ), and b) vertical velocity climatology  $\bar{\omega}$  (bluegreen  
 432 line:  $10^{-2} Pa.s^{-1}$ ), MSE anomaly  $m'$  (line with stars:  $10^3 J.Kq^{-1}$ ), enthalpy anomaly  $c_p T'$  (line  
 433 with squares:  $10^3 J.Kq^{-1}$ ), latent energy anomaly  $l_v q'$  (line with triangles:  $10^3 J.Kq^{-1}$ ) and  
 434 geopotential anomaly  $\Psi'$  (line with dark circle:  $10^3 J.Kq^{-1}$ ) averaged over the Northern part of  
 435 West Central Africa (6°N-14°N, 6°-20°E) and c), d) the same parameters averaged over the  
 436 Southern part of West Central Africa (6°S-5°N, 6°-20°E) during October 2019.

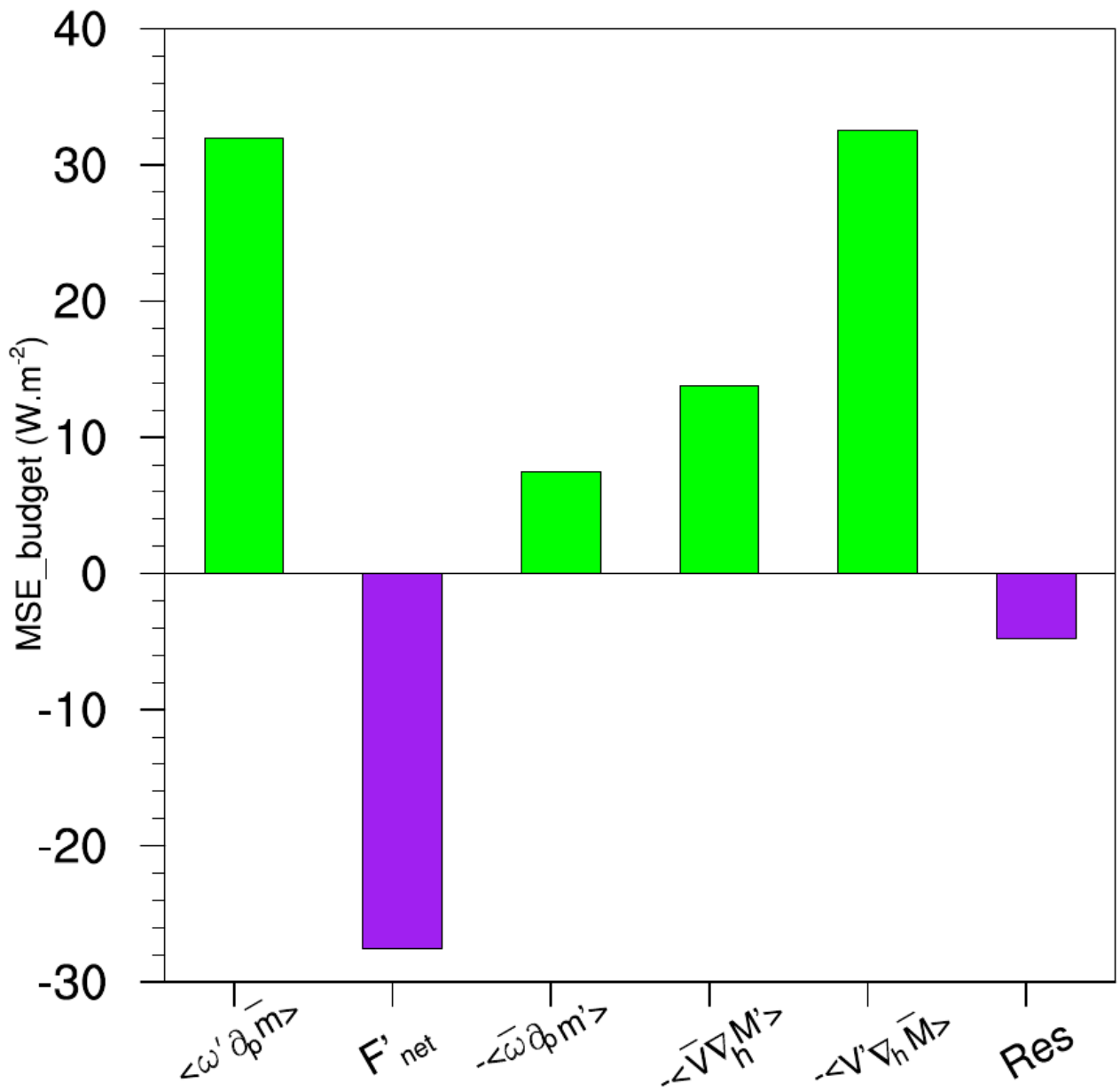
437

438 values from 900 hPa up to the upper troposphere, accelerating the anomalous vertical movement.  
 439 The structure of the MSE climatology is similar to that observed to the north, with a maximum of  
 440 around 650 hPa. The vertical profiles (Fig. 8d) of the MSE anomaly and the latent energy anomaly  
 441 show similar structures throughout the tropospheric column, with maximum values at 650 hPa.

442 The vertical velocity anomaly  $\omega'$  shows positive values at the surface and negative values in the  
 443 middle and upper troposphere. The alternation of positive and negative values in the tropospheric  
 444 column probably reduces the contribution of the vertical advection of moisture induced by the  
 445 anomalous vertical motion. The MSE climatology  $\bar{m}$  exhibits a bottom-heavy bove structure with a  
 446 maximum around 650 hPa. Such a structure generally indicates that  $\langle \partial_p \bar{m} \rangle < 0$  (Chen and Bordoni,  
 447 2014; Liu et al. 2021; Wen et al. 2022). As a result, positive (negative) values of  $\langle \omega' \partial_p \bar{m} \rangle$  indicate

448 anomalous ascending (descending) motion over West Central Africa. The vertical velocity  
449 climatology  $\bar{\omega}$  (Fig. 6b) is negative over the entire troposphere, characterizing an upward  
450 movement. The MSE anomaly  $m'$  decreased near the surface then increased from 800 hPa to 550  
451 hPa, with a maximum value around 650 hPa. However, this includes three terms, namely,  $gz'$  -  
452 which is weak in the entire tropospheric column, the enthalpy anomaly  $c_p T'$ , which tends to  
453 increase, and  $l_v q'$ , which approaches  $m'$  :

454 Based on the contributions of the different terms in equation 9 to the MSE over the northern  
455 part of averaged over West Central Africa (Fig. 97), the advection of wet enthalpy induced by the  
456 horizontal wind anomalies  $-\langle \mathbf{V}' \cdot \nabla M \rangle$  is the main term contributing most to the vertical  
457 advection of the MSE induced by the vertical velocity anomaly  $\langle \omega' \partial_p \bar{m} \rangle$ . This is confirmed by the  
458 high correlation (r = 0.6) between the two terms compared to the other terms.



459

460 **Fig. 7.** Different terms of the Moist Static Energy (MSE) budget averaged over West Equatorial  
 461 Africa.

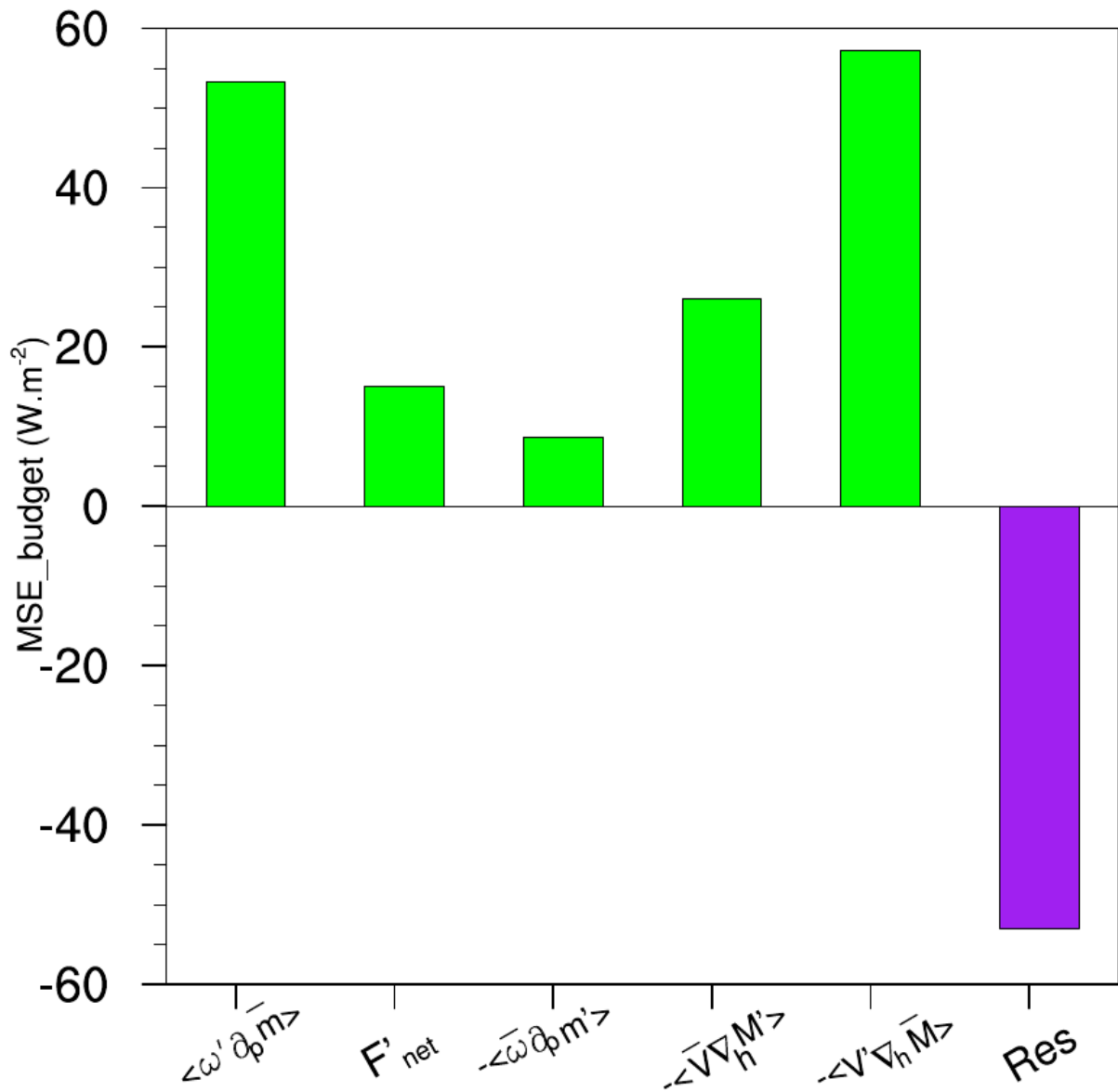
462

463 We also note the contribution of the thermodynamic terms, although the horizontal advection of the  
 464 MSE induced by the wet enthalpy variation  $-\langle \bar{V} \cdot \nabla_h M' \rangle$  dominates compared to the vertical  
 465 advection of the MSE induced by the MSE variation  $-\langle \omega \partial_p m' \rangle$ . A reduction in the net energy  
 466 flux is noticeable. This could be due to the fact that the energy in the radiative and turbulent heat  
 467 fluxes penetrating the atmosphere over West central Africa has suffered a loss linked to the increase  
 468 in cloud cover, which has a strong influence on short-wave radiation. Such a reduction in energy in-



469 the air column has an impact on upward motion. This result is in line with that of Wen et al. (2022)  
 470 and Sheng et al. (2023), who pointed to a reduction in the net energy in the air column during the  
 471 exceptional rainy season in the summer of 2020 in the Yangtze river valley and the anomalous  
 472 increase in precipitation over southern China in 2022. However, the residual term is weak.

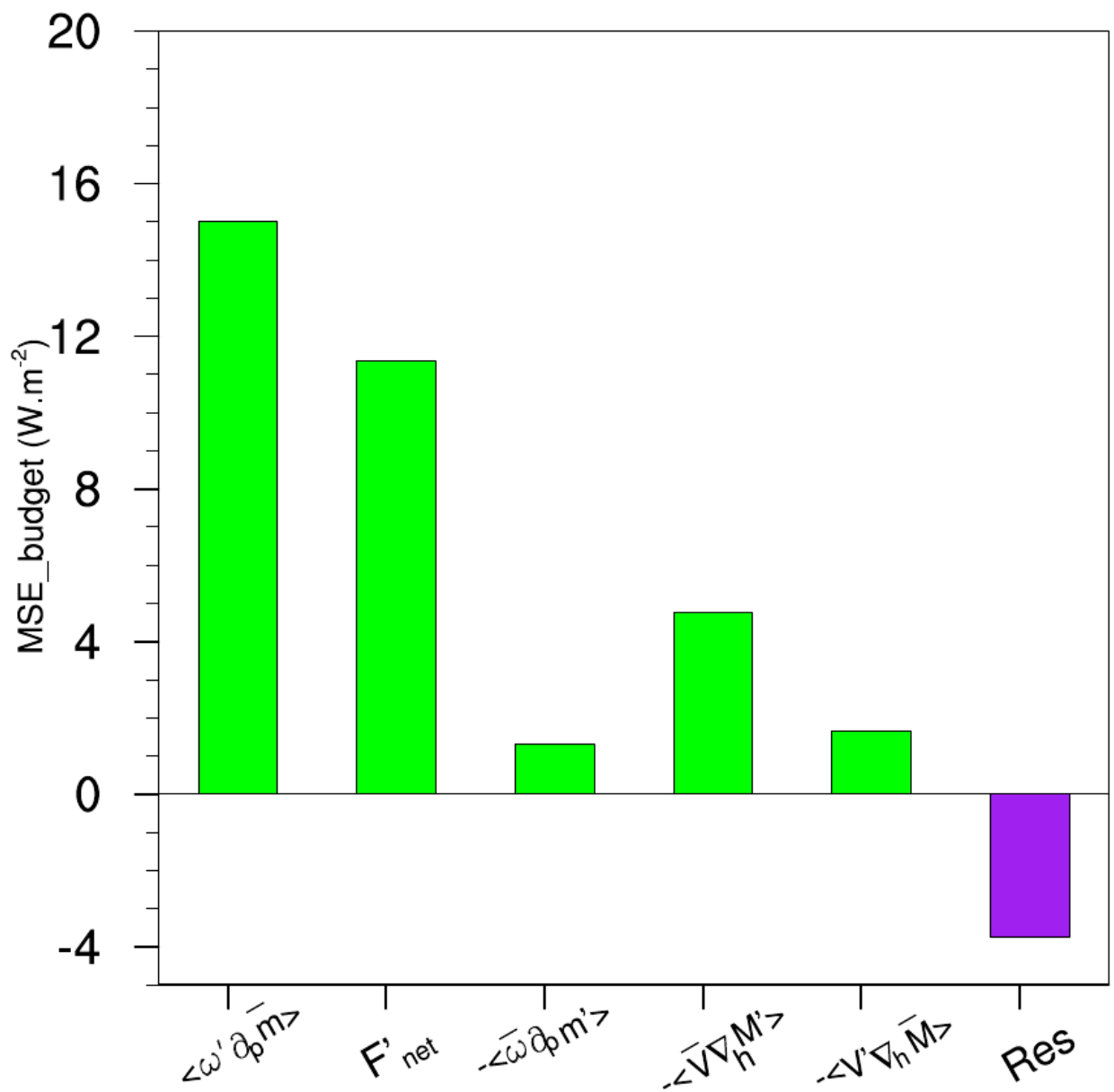
473 — On a regional scale, the vertical advection of the MSE induced by the vertical motion anomaly  
 474  $\langle \omega' \partial_p \bar{m} \rangle$  (Fig. 8a) is mainly dominated by the dynamic term  $-\langle \mathbf{V}' \cdot \nabla M \rangle$  (Fig. 8c), which brings  
 475 moist enthalpy into the domain.



476  
 477 **Fig. 9.** Different terms of the Moist Static Energy (MSE) budget averaged over the Northern part of  
 478 West Central Africa (6°N-14°N, 6°-20°E).

479 | We also note the contribution of the thermodynamic terms, although the horizontal advection of the  
480 | MSE induced by the wet enthalpy variation  $-\langle \nabla \cdot \nabla M' \rangle$  dominates ( $r = 0.3$ ) compared to the  
481 | vertical advection of the MSE induced by the MSE variation  $-\langle \omega \partial_p m' \rangle$  ( $r = -0.2$ ). A weak  
482 | contribution from the net flow of energy is noticeable ( $r = 0.18$ ). This could be due to the fact that  
483 | the energy in the radiative and turbulent heat fluxes penetrating the atmosphere over West Central  
484 | Africa has suffered a loss linked to the increase in cloud cover, which has a strong influence on

485 | short-wave radiation. Such a reduction in energy in the air column has an impact on upward motion.



486

487 **Fig. 10.** Different terms of the Moist Static Energy (MSE) budget averaged over the Southern part of  
 488 West Central Africa (6°S-5°N, 6°-20°E).

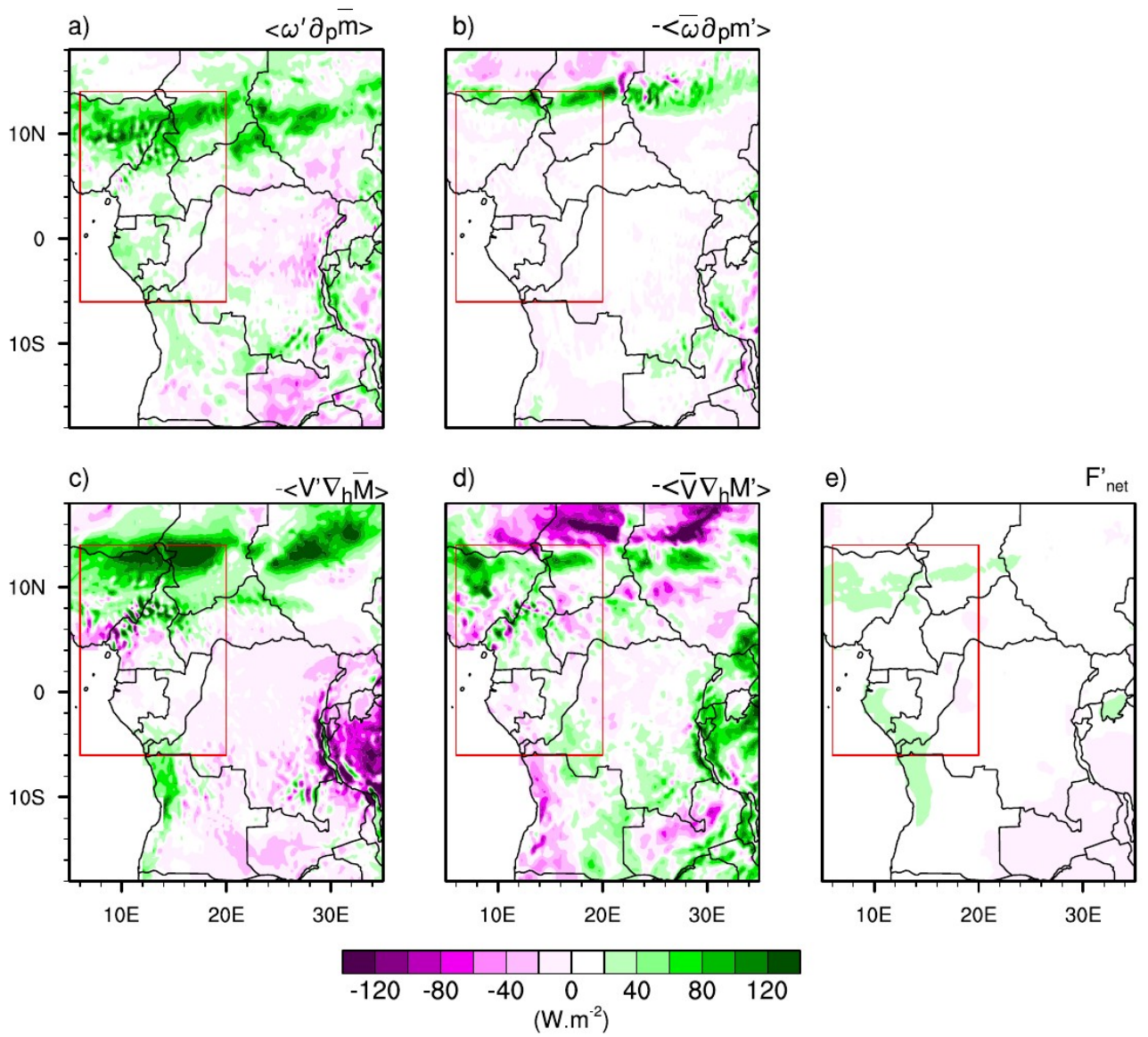
489

490 This result is in line with that of Wen et al. (2022) and Sheng et al. (2023), who pointed to a  
 491 reduction in the net energy in the air column during the exceptional rainy season in the summer of  
 492 2020 in the Yangtze River valley and the anomalous increase in precipitation over southern China  
 493 in 2022. However, as with the moisture balance, the residual term is also considerable.

494 To the south of the domain(Fig. 10), the increase in the net energy balance was responsible for  
 495 strengthening the vertical advection of the MSE induced by the vertical velocity anomaly (r = 0.51).  
 496 In addition, the increase in vertical movement was reinforced by an increase in the horizontal

497 | advection of the MSE induced by the variation in wet enthalpy  $-\langle \mathbf{V} \cdot \nabla M' \rangle$ . This is in agreement  
498 | with the results of Kenfack et al. (2024) who highlighted the importance of horizontal advections in  
499 | the MSE and moisture flux as well as their implications for vertical motion over the Congo Basin.  
500 | The contributions in vertical advection induced by changes in the MSE and horizontal advection  
501 | induced by changes in the horizontal wind are small. Moreover, similarly to the moisture flux  
502 | advected in the western part of the Congo Basin, the residual term was less important in the MSE  
503 | budget compared to the northern part.

504 | On a regional scale, the vertical advection of the MSE induced by the vertical motion anomaly  
505 |  $\langle \omega' \partial_p \bar{m} \rangle$  (Fig. 11a) is mainly dominated by the dynamic term  $-\langle \mathbf{V}' \cdot \nabla \bar{M} \rangle$  (Fig. 11c), which



508 **Fig. 118.** Spatial distributions of each term of the Moist Static Energy (MSE) balance equation  
 509 during October 2019 over West Equatorial Africa (Red box). (a) vertical advection of climatological  
 510 MSE by anomalous vertical velocity, (b) vertical advection of anomalous MSE by climatological  
 511 vertical velocity, (c) horizontal advection of anomalous moist enthalpy by climatological wind, (e)  
 512 horizontal advection of climatological moist enthalpy by anomalous wind, and (f) net energy flux (at  
 513 the surface and top of the atmosphere) in the atmospheric column.

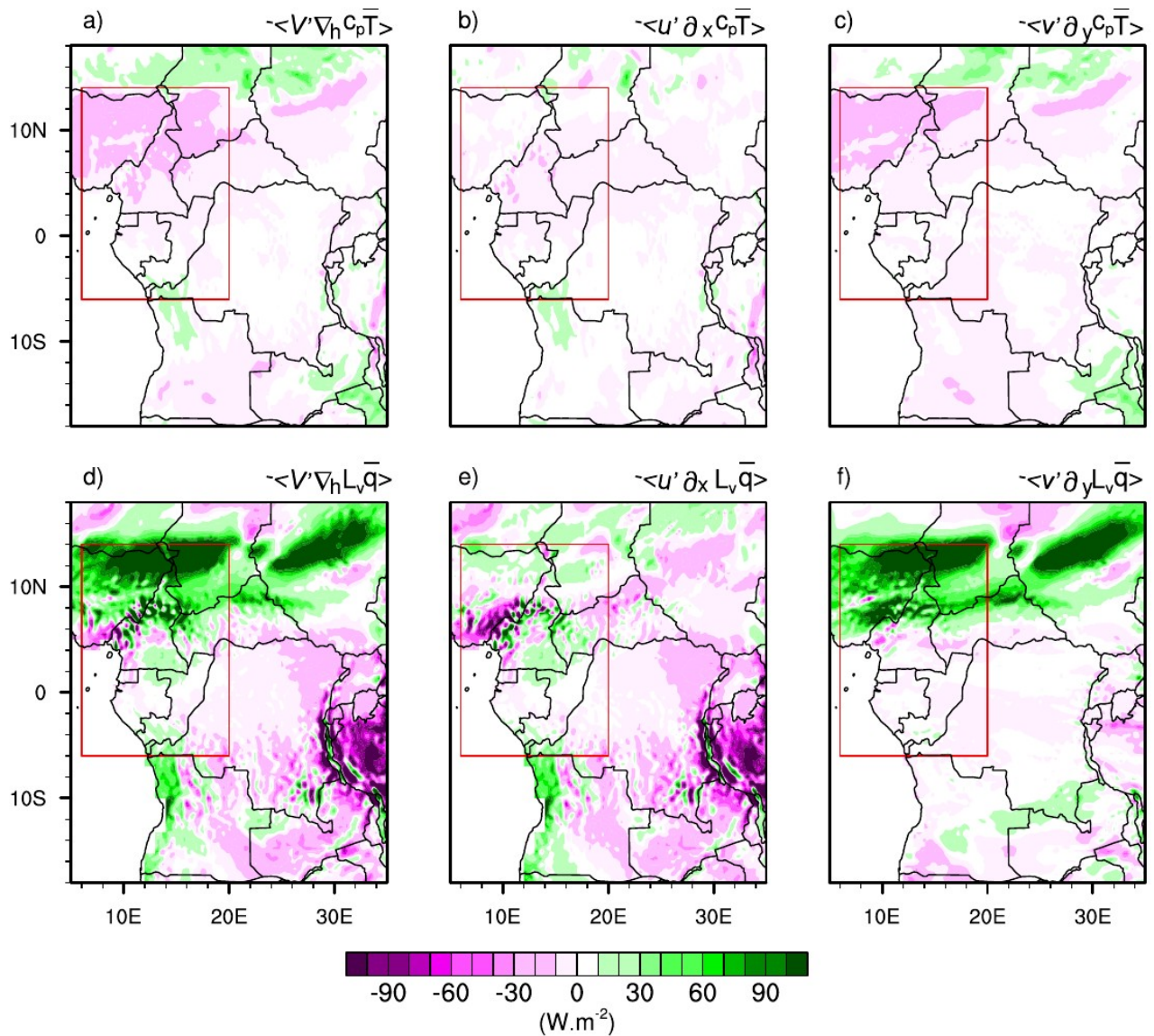
514

515 There is a high concentration of positive values in both dynamic terms, up to  $120 \text{ W}\cdot\text{m}^{-2}$  in the  
 516 north of West Central Africa. In addition, the two thermodynamic terms  $-\langle \omega \partial_p m' \rangle$  (Fig. 11b8b)  
 517 and  $-\langle \nabla \cdot \nabla M' \rangle$  (Fig. 11d8d), although weak, also contributed to reinforcing the vertical  
 518 advection of MSE induced by the vertical motion anomaly. It should be remembered that the term  
 519  $-\langle \omega \partial_p m' \rangle$  remains very weak over the region as a whole, except the with the exception of the  
 520 northern part where a slight layer of positive values can be observed. Terms  $-\langle \mathbf{V}' \cdot \nabla M \rangle$ ,  
 521  $-\langle \nabla \cdot \nabla M' \rangle$  and  $-\langle \omega \partial_p m' \rangle$  in the MSE have a similar spatial distribution to terms  
 522  $\langle -\mathbf{V}' \cdot \nabla \bar{q} \rangle$ ,  $\langle -\nabla \cdot \nabla q' \rangle$  and  $\langle -\bar{\omega} \partial_p q' \rangle$  in the moisture, which is in agreement with the  
 523 findings of Kenfack et al. (2024). The difference between the net energy balance for 2019 and the  
 524 climatology (Fig. 11e8e) shows low positive values in the north and south negative values for the  
 525 whole of the region respectively. Such an increase (mainly to the south of the area) is associated  
 526 with a strengthening. The MSE balance indicates a pronounced net energy reduction in the  
 527 atmospheric column over the Sahel, which results in a decrease in the vertical structure of the MSE  
 528 anomaly through ascending currents and, consequently, an increase in precipitation advection of  
 529 moisture induced by the anomalous vertical motion. Although the dynamic contribution is the most  
 530 important, the thermodynamic contribution cannot be neglected. This would mean that the  
 531 interaction feedbacks between atmospheric dynamic and thermodynamic variables would induce  
 532 significant indirect effects on October 2019 precipitation anomalies over West Central Africa.

### 533 5.1 Dynamic effect

534 The aforementioned results clearly show that enthalpy advection induced by the horizontal wind  
 535 anomaly is crucial in understanding the processes at the origin of October 2019 extreme  
 536 precipitation over northern part of West Central Africa. It should be remembered that, as we  
 537 mentioned in the diagnostic section of the MSE balance, the wet enthalpy  $M = c_p T + L_v q$  results

538 from the sum of the dry enthalpy and the latent heat. Thus, the horizontal advection of wet enthalpy  
 539 induced by the wind anomaly can be separated into two terms: dry enthalpy  $-\langle \mathbf{V}' \cdot \nabla_h c_p T \rangle$  (Fig.  
 540 [12a9a](#)) and latent heat  $-\langle \mathbf{V}' \cdot \nabla_h l_v \bar{q} \rangle$  (Fig. [12d9d](#)).



541

542 **Fig. 129.** Horizontal advection of (a–c) climatological dry enthalpy and (d–f) latent energy by  
 543 anomalous wind, designated as a dynamic effect during October 2019 over West Central Africa  
 544 ([Red box](#)). (a, d) Total advection, (b, e) zonal component, and (c, f) meridional component.

545

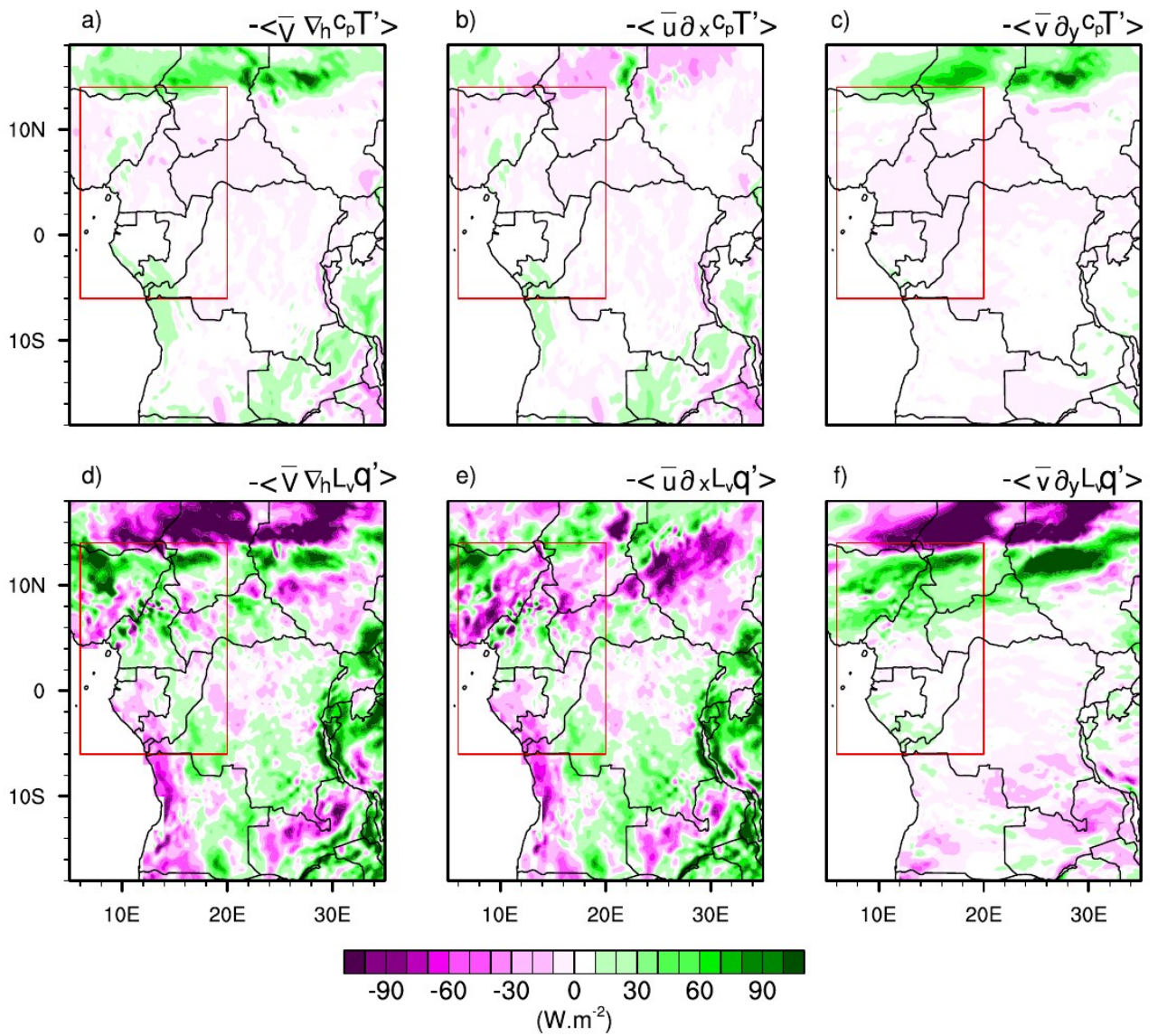
546 Given the influence of the wind anomaly components on the displacement of dry enthalpy and  
 547 latent heat, a further decomposition of the  $-\langle \mathbf{V}' \cdot \nabla_h c_p T \rangle$  and  $-\langle \mathbf{V}' \cdot \nabla_h l_v \bar{q} \rangle$  terms along the  
 548 zonal (Figs. [12b9b,e](#)) and meridional (Figs. [12c9e,f](#)) directions [appear](#) necessary. Figure



549 [12a9a](#) shows that the advection of dry enthalpy induced by the horizontal wind anomaly decreased  
550 over the ~~area-averaged entire domain~~, with the highest values between 6°N and 14°N. The advection  
551 of dry enthalpy by the meridional wind anomaly (Fig. [12c9e](#)) is particularly responsible for the  
552 decrease in the  $-\langle \mathbf{V}' \cdot \nabla_h c_p T' \rangle$  term compared with the advection of dry enthalpy induced by the  
553 zonal wind anomaly (Fig. [12b9b](#)), which is weak. For the transport of latent heat (Fig. [12d9d](#)), the  
554 influence of the advection of  $-\langle \mathbf{V}' \cdot \nabla_h l_v \bar{q} \rangle$  term under the effect of the anomalous meridional  
555 circulation is the main term responsible for the supply of moist air to the northern part of the area,  
556 while the low contribution to the south is associated with a low input of moist air from the zonal  
557 wind anomaly (Fig. [12f9f](#)). Analysis of the advection of dry enthalpy and latent heat by anomalous  
558 winds shows that the meridional wind anomaly had a significant impact compared with the zonal  
559 wind anomaly. In addition, the advection of the dynamic term associated with latent heat  
560 contributed significantly to the supply of ~~MSE moist air~~ to West Central Africa compared to the  
561 advection of the dynamic term associated with dry enthalpy. One of the reasons would be because  
562 in addition to the warm Atlantic SSTs, there was also an anomalous meridional mean sea level  
563 pressure (MSLP) gradient in the Central African Sahel between a lower MSLP over the eastern  
564 Sahara and a higher pressure between 10 and 15°N. In addition, the trans-equatorial meridional  
565 wind fluctuated with the activity of the African easterly waves over the Gulf of Guinea (Nicholson  
566 et al. 2022).

## 567 5.2 Thermodynamic effect

568 The results of the previous section highlighted the importance of dynamics, particularly in a  
569 meridional direction, on extreme precipitation in October 2019. However, we previously also  
570 observed that the thermodynamic contribution should not be neglected. ~~(Fig. 8d).~~ Similar to the  
571 previous section, the thermodynamic term  $-\langle \nabla \cdot \nabla M' \rangle$  (i.e. the advection of the wet enthalpy  
572 anomaly associated with wind climatology) can also be separated into two terms, namely: Dry  
573 enthalpy  $-\langle \nabla \cdot \nabla_h c_p T' \rangle$  (Fig. [13a10a](#)) and latent heat  $-\langle \nabla \cdot \nabla_h l_v \bar{q}' \rangle$  (Fig. [13d10d](#)).



574

575 **Fig. 1310.** As in Fig. 129, but for the thermodynamic effect (horizontal advection of anomalous dry  
 576 enthalpy and latent energy by climatological wind) during October 2019 over West Central Africa  
 577 (Red box).

578

579 To better assess the contribution of each term, we split the horizontal wind into zonal and  
 580 meridional directions. The advection of the dry enthalpy anomaly by the horizontal zonal and  
 581 meridional wind components is shown in Figures 13b and 13c and 10b and 10e, respectively. It can  
 582 also be seen that the dry enthalpy anomaly is very small over the whole area. On the other hand, the  
 583 advection of the latent heat anomaly by the horizontal wind climatology is more pronounced.  
 584 Variations in latent heat are strong in the meridional direction, while the zonal direction shows a  
 585 reduction in abnormal latent heat. This could be due to the strong meridional wind associated with

586 | ~~the increase in SST in the tropical~~warming-of-the-equatorial Atlantic, which results in strong  
587 advection of water vapor into West Central Africa, leading to precipitation. The reduction in  
588 advection of the latent heat anomaly on the Atlantic coast is amplified by the zonal wind  
589 climatology. However, the advection of the wet enthalpy induced by the horizontal wind anomaly  
590 (dynamic effect) is stronger than the advection of the wet enthalpy anomaly by the wind  
591 climatology. As a result, we note in particular the changes in the meridional wind for the dynamic  
592 effect and the latent heat associated with the warming of the equatorial Atlantic for the  
593 thermodynamic effect.

## 594 **6 Summary and concluding remarks**

595 West Central Africa was hit by unprecedented exceptional rainfall in October 2019. A few  
596 studies have investigated the meteorological causes associated with these extreme rainfall events  
597 (Wainwright et al, 2020; Nicholson et al. 2022). This study followed these perspectives and focused  
598 on evaluating the dynamic and thermodynamic processes that controlled the extreme events of  
599 2019. We proceeded by decomposing the water balance and MSE equation, separating the  
600 associated dynamic and thermodynamic effects. Changes in atmospheric circulation are behind  
601 dynamic processes, while changes in water vapor are behind thermodynamic processes. This  
602 approach provides a better understanding of the mechanisms behind rainfall anomalies. The  
603 thermodynamic effect, in particular, can be ~~used to speculate on the influence~~exploited-to-estimate-  
604 ~~the impact~~ of global warming on ~~heavy rainfall in~~the-heavy-precipitation-of October 2019, notably  
605 on the increase in the temperature of the troposphere and its water vapor content. The main findings  
606 can be ~~summarised~~summarized as follows:

- 607 | 1. The main feature of October 2019 ~~in the northern part of the area~~ was a strong southerly  
608 circulation compared with the typical climatology for 1988-2017. In addition, a more  
609 pronounced rate of humidity associated with significant diabatic heating over West Central  
610 Africa up to 15°N ~~was~~were recorded.
- 611 | 2. The diagnosis of the water balance reveals that the exceptional rainfall in October 2019  
612 ~~was~~is mainly dominated by dynamic effects. However, moisture advection induced by  
613 horizontal wind anomalies ~~is the dominant process of~~controls-precipitation anomalies ~~over~~  
614 ~~the northern part in the north~~of the ~~zone~~area, while vertical moisture advection induced by  
615 vertical velocity anomalies ~~is the dominant process of~~controls-precipitation extremes in the  
616 south, mainly over Gabon and southern Congo Brazzaville. Changes in the thermodynamic  
617 effect, although not the key factor responsible for the events of October 2019, contribute up

618 to 3527.5% of the total effect (the sum of the dynamic and thermodynamic contributions) on  
619 the northern part and 15% on the southern part of the domain. The contribution of  
620 evaporation remains weak in both areas combined, which allows us to conclude that  
621 evaporation was not responsible for the heavy rainfall of October 2019 in West Central  
622 Africa.

623 3. The MSE vertical advection anomaly is dominated over the northern part of the area of the  
624 MSE was controlled by the dynamic term (i.e. the advection of the wet enthalpy induced by  
625 the horizontal wind anomalies) compared to the thermodynamic terms (i.e. the horizontal  
626 advection of the MSE induced by the variation of the wet enthalpy and the vertical  
627 advection of the MSE induced by the variation of the MSE). In the southern part, the  
628 increase in the net energy balance compared with the climatology is the dominant process  
629 that has contributed most to the change in the structure of the vertical anomaly of the MSE.  
630 An extended analysis shows that these ~~These~~ variations in the MSE over the north of West  
631 Central Africa were governed by its meridional component, in particular the variations in  
632 the meridional wind in the dynamic effect and the meridional variations in latent heat in the  
633 thermodynamic effect. It should be pointed out that in both cases, the contribution of dry  
634 enthalpy helped to reduce the dynamic term and was small in the thermodynamic term.

635 The results of this study show that moisture advection induced by horizontal wind anomalies and  
636 vertical moisture advection induced by vertical velocity anomaly were crucial mechanisms ~~in~~ the  
637 anomalous October 2019 exceptional rainfall increase over West Central Africa. In addition,  
638 changes in the MSE budget, mainly through the meridional circulation (dynamic effect), and latent  
639 heat (thermodynamic effect) also played an important role in the northern part of the area, while the  
640 increase in the energy balance contributed considerably to the change in the MSE balance in the  
641 southern part of the area. However, there was little contribution from dry enthalpy. These results are  
642 consistent with those of Nicholson et al (~~2022~~2024) who showed that the increase in equatorial  
643 Atlantic SSTs associated with the late retreat of the West African monsoon played an important role  
644 in precipitation anomalies in the Sahel. Changes in SSTs along the east coast of the equatorial  
645 Atlantic display a similar pattern to the Atlantic Niño as described by Lutz et al. (2013).  
646 Furthermore, Vallès-Casanova et al (2020) also highlighted the fact that 2019 was characterised by  
647 a particularly intense Atlantic Niño, which lasted until October, placing the dynamic and  
648 thermodynamic processes in the context of the large-scale circulation. The importance of the  
649 dynamic contribution during extreme precipitation events has been reported in other regions,  
650 notably over southern China (Wen et al. 2022; Sheng et al. 2023). This calls for comprehensive

651 evaluations of both dynamic and thermodynamic contributions, and their possible feedback, to  
652 assess the potential impact of climate change on extreme precipitation events in this region.

653

654 **Acknowledgements.** The authors thank all the observational and reanalysis data providers used in  
655 this study, and the research of the International Joint Laboratory “Dynamics of Terrestrial  
656 Ecosystems in Central Africa: A Context of Global Changes” (IJL DYCOCA/LMI DYCOFAC).

657

658 **Competing Interests.** The authors declare that they have no conflict of interest.

659

#### 660 **Authors' contributions**

661 **kevin Kenfack:** Conceptualization; data analysis; formal analysis; investigation; methodology;  
662 writing - original draft; review and editing.

663 **Francesco Marra:** Supervision; conceptualization; investigation; writing – review and editing.

664 **Zéphirin Yepdo Djomou:** Investigation; writing; review and editing; supervision; validation.

665 **Lucie A. Djotang Tchotchou:** Validation; supervision; methodology; writing – review and editing.

666 **Alain T. Tamoffo:** Conceptualization; investigation; methodology; project administration; resources;  
667 supervision; validation; review and editing.

668 **Derbetini A. Vondou:** Project administration; supervision; resources; validation; methodology;  
669 writing – review and editing.

670

671 **Funding.** Not applicable

672

#### 673 **Data Availability Statement**

674

675 The **ERA5** reanalysis is produced within the Copernicus Climate Change Service (C3S) by the  
676 ECMWF and is accessible via the link [https://cds.climate.copernicus.eu/cdsapp#!/dataset/reanalysis-  
677 era5-pressure-levels-monthly-means?tab1/4form](https://cds.climate.copernicus.eu/cdsapp#!/dataset/reanalysis-era5-pressure-levels-monthly-means?tab1/4form).

678

679 |

#### 680 | **References**

681

682  
683 Andrews, P. C., Cook, K. H., ~~and~~ Vizy, E. K.: ~~(2023)~~. Mesoscale convective systems in the Congo  
684 Basin: Seasonality, regionality, and diurnal cycles, ~~*Clim. Dynam.*, 62.~~ ~~*Climate Dynamics*, 62(1)~~,  
685 609–630. ~~;~~ <https://doi.org/10.1007/s00382-023-06903-7>, ~~2023~~.  
686  
687 ~~[Kenya – over 100 dead, 18,000 displaced after recent floods and landslides – floodlist:](http://floodlist.com/africa/kenya-floods-november-2019)~~  
688 ~~<http://floodlist.com/africa/kenya-floods-november-2019>, last access: 2 April 2024.~~  
689  
690 Aretouyap, Z., Kemgang, F. E. G., Domra, J. K., Bisso, D., ~~and~~ Njandjock, P. N.: ~~(2021)~~.  
691 Understanding the \_\_\_ occurrences of fault and landslide in the region of West-Cameroon using  
692 remote sensing and GIS techniques, ~~*Nat.*~~ ~~*Natural Hazards*, 109(2)~~, 1589–1602. ~~;~~  
693 <https://doi.org/10.1007/s11069-021-04890-8>, ~~2021~~.  
694  
695 Bell, J. P., Tompkins, A. M., Bouka-Biona, C., ~~and~~ Sanda, I. S.: ~~(2015)~~. A process-based  
696 investigation into the impact of the Congo basin deforestation on surface climate, ~~*J. Geophys. Res-*~~  
697 ~~*Atmos.*, 120.~~ ~~*Journal of Geophysical Research: Atmospheres*, 120(12)~~, 5721–5739. ~~;~~  
698 <https://doi.org/10.1002/2014jd022586>, ~~2015~~.  
699  
700 Black, E.: ~~(2005)~~. The relationship between Indian Ocean sea–surface temperature and East African  
701 rainfall, ~~*Philos. T. R. Soc. A*, 363.~~ ~~*Philosophical Transactions of the Royal Society A: Mathematical,*~~  
702 ~~*Physical and Engineering Sciences*, 363(1826)~~, 43–47. ~~;~~ <https://doi.org/10.1098/rsta.2004.1474>, ~~2005~~.  
703  
704 Chadwick, R., Good, P., ~~and~~ Willett, K.: ~~(2016)~~. A simple moisture advection model of specific  
705 humidity change over land in response to SST warming, ~~*J.*~~ ~~*Journal of Climate*, 29(21)~~, 7613–7632. ~~;~~  
706 <https://doi.org/10.1175/jcli-d-16-0241.1>, ~~2016~~.  
707  
708 Chen, J. ~~and~~ ~~&~~ Bordoni, S.: ~~(2014)~~. Orographic effects of the Tibetan plateau on the east Asian  
709 summer monsoon: An energetic perspective, ~~*J.*~~ ~~*Journal of Climate*, 27(8)~~, 3052–3072. ~~;~~  
710 <https://doi.org/10.1175/jcli-d-13-00479.1>, ~~2014~~.  
711  
712 Cook, K. H. ~~and~~ ~~Liu, Y., &~~ Vizu, E. K.: ~~Hydrodynamics of regional and seasonal variations in~~  
713 ~~*Congo Basin precipitation*, *Clim. Dynam.*, 59, 1775–1797.~~ ~~(2019)~~. Congo Basin drying associated  
714 ~~with poleward shifts of the African thermal lows.~~ ~~*Climate Dynamics*, 54(1–2)~~, 863–883.  
715 <https://doi.org/10.1007/s00382-021-06066-3>, ~~2021.019-05033-3~~

716

717 Cook, K. H., [Liu, Y., and Vizy, E. K.:](#) [Congo Basin drying associated with poleward shifts of the](#)  
718 [African thermal lows, \*Clim. Dynam.\*, 54, 863–883, \(2021\).](#) ~~Hydrodynamics of regional and seasonal~~  
719 ~~variations in Congo Basin precipitation. *Climate Dynamics*, 59(5–6), 1775–1797.~~  
720 <https://doi.org/10.1007/s00382-019-05033-3>, [2019.021-06066-3](#)

721

722 Dyer, E. L. E., Jones, D. B. A., Nusbaumer, J., Li, H., Collins, O., Vettoretti, G., [and Noone, D.:](#)  
723 ~~(2017).~~ Congo Basin precipitation: Assessing seasonality, regional interactions, and sources of  
724 moisture, [J. Geophys. Res-Atmos.](#), ~~122.~~ [Journal of Geophysical Research: Atmospheres](#), ~~122(13),~~  
725 ~~6882–6898.~~ <https://doi.org/10.1002/2016jd026240>, [2017.](#)

726

727 Fontaine, B., Roucou, P., [and Trzaska, S.:](#) ~~(2003).~~ Atmospheric water cycle and moisture fluxes in  
728 the West African monsoon: Mean annual cycles and relationship using NCEP/NCAR reanalysis,  
729 [Geophys. Res. Lett.](#), ~~30.~~ [Geophysical Research Letters](#), ~~30(3).~~  
730 <https://doi.org/10.1029/2002gl015834>, [2003.](#)

731

732 Fotso-Nguemo, T. C., Chamani, R., Yepdo, Z. D., Sonkoué, D., Matsaguim, C. N., Vondou, D. A.,  
733 [and Tanessong, R. S.:](#) ~~(2018).~~ Projected trends of extreme rainfall events from CMIP5 models over  
734 Central Africa, [Atmos. Sci. Lett.](#), ~~19.~~ [Atmospheric Science Letters](#), ~~19(2).~~  
735 <https://doi.org/10.1002/asl.803>, [2018.](#)

736

737 Fotso-Nguemo, T. C., Diallo, I., Diakhaté, M., Vondou, D. A., Mbaye, M. L., Haensler, A., Gaye, A.  
738 T., [and Tchawoua, C.:](#) ~~(2019).~~ Projected changes in the seasonal cycle of extreme rainfall events  
739 from CORDEX simulations over Central Africa, [Climatic.](#) ~~Climatic~~ Change, ~~155(3),~~ 339–357,  
740 <https://doi.org/10.1007/s10584-019-02492-9>, [2019.](#)

741

742 Funk, C., Peterson, P., Landsfeld, M., Pedreros, D., Verdin, J., Shukla, S., Husak, G., Rowland, J.,  
743 Harrison, L., Hoell, A., [and Michaelsen, J.:](#) ~~(2015).~~ The climate hazards infrared precipitation with  
744 stations—a new environmental record for monitoring extremes, [Scientific Data](#), ~~2,(1).~~  
745 <https://doi.org/10.1038/sdata.2015.66>, [2015.](#)

746

747 Garcin, Y., Deschamps, P., Ménot, G., de Saulieu, G., Schefuß, E., Sebag, D., Dupont, L. M.,  
748 Oslisly, R., Brademann, B., Mbusnum, K. G., Onana, J.-M., Ako, A. A., Epp, L. S., Tjallingii, R.,  
749 Strecker, M. R., Brauer, A., [and Sachse, D.:](#) ~~(2018).~~ Early anthropogenic impact on Western

750 Central African rainforests 2,600 y ago, *P. Natl. A. Sci. India. A*, *115*, *Proceedings of the National*  
751 *Academy of Sciences*, *115(13)*, 3261–3266, <https://doi.org/10.1073/pnas.1715336115>, *2018*.

752

753 Gou, Y., Balling, J., De Sy, V., Herold, M., De Keersmaecker, W., Slagter, B., Mullissa, A., Shang,  
754 X., *and* Reiche, J.: *(2022)*. Intra-annual relationship between precipitation and forest disturbance in  
755 the African rainforest, *Environ. Res. Lett.*, *17*, 044044, *Environmental Research Letters*, *17(4)*,  
756 *044044*. <https://doi.org/10.1088/1748-9326/ac5ca0>, *2022*.

757

758 Harris, I., Osborn, T. J., Jones, P., *and* Lister, D.: *(2020)*. Version 4 of the CRU TS monthly high-  
759 resolution gridded multivariate climate dataset, *Scientific Data*, *7*, *(1)*.  
760 <https://doi.org/10.1038/s41597-020-0453-3>, *2020*.

761

762 He, Y., Tian, W., Huang, J., Wang, G., Ren, Y., Yan, H., Yu, H., Guan, X., *and* Hu, H.: *(2021)*.  
763 The mechanism of increasing summer water vapor over the Tibetan plateau, *J. Geophys. Res-Atmos.*,  
764 *126*, *Journal of Geophysical Research: Atmospheres*, *126(10)*.  
765 <https://doi.org/10.1029/2020jd034166>, *2021*.

766

767 Hersbach, H., Bell, B., Berrisford, P., Hirahara, S., Horányi, A., Muñoz-Sabater, J., Nicolas, J.,  
768 Peubey, C., Radu, R., Schepers, D., Simmons, A., Soci, C., Abdalla, S., Abellan, X., Balsamo, G.,  
769 Bechtold, P., Biavati, G., Bidlot, J., Bonavita, M., *De Chiara, G., Dahlgren, P., Dee, D., Diamantakis,*  
770 *M., Dragani, R., Flemming, J., Forbes, R., Fuentes, M., Geer, A., Haimberger, L., Healy, S., Hogan,*  
771 *R. J., Hólm, E., Janisková, M., Keeley, S., Laloyaux, P., Lopez, P., Lupu, C., Radnoti, G., de Rosnay,*  
772 *P., Rozum, I., Vamborg, F., Villaume, S., and ...*Thépaut, J.: *(2020)*. The ERA5 global reanalysis,  
773 *Q. J. Roy. Meteor. Soc.*, *146*, *Quarterly Journal of the Royal Meteorological Society*, *146(730)*,  
774 1999–2049, <https://doi.org/10.1002/qj.3803>, *2020*.

775

776 Hua, W., Zhou, L., Nicholson, S. E., Chen, H., *and* Qin, M.: *(2019)*. Assessing reanalysis data for  
777 understanding rainfall climatology and variability over Central Equatorial Africa, *Clim. Dynam.*, *53*,  
778 *Climate Dynamics*, *53(1–2)*, 651–669, <https://doi.org/10.1007/s00382-018-04604-0>, *2019*.

779

780 Huffman, G. J., Adler, R. F., Bolvin, D. T., *and* Gu, G.: *(2009)*. Improving the global precipitation  
781 record: GPCP Version 2.1, *Geophys. Res. Lett.*, *36*, *Geophysical Research Letters*, *36(17)*.  
782 <https://doi.org/10.1029/2009gl040000>, *2009*.

783



784 Jackson, B., Nicholson, S. E., ~~and~~ Klotter, D.: ~~(2009)~~. Mesoscale convective systems over Western  
785 Equatorial Africa and their relationship to large-scale circulation, ~~Mon. Weather. Rev., 137. Monthly~~  
786 ~~Weather Review, 137(4)~~, 1272–1294. ~~https://doi.org/10.1175/2008mwr2525.1, 2009.~~  
787

788 Jiang, J., Zhou, T., Chen, X., ~~and~~ Zhang, L.: ~~(2020)~~. Future changes in precipitation over Central  
789 Asia based on CMIP6 projections, ~~Environ. Res. Lett., 15, 054009. Environmental Research Letters,~~  
790 ~~15(5), 054009.~~ ~~https://doi.org/10.1088/1748-9326/ab7d03, 2020.~~  
791

792 Johannsen, Ermida, Martins, Trigo, Nogueira, ~~and Dutra: & Dutra.~~ ~~(2019)~~. Cold bias of ERA5  
793 summertime daily maximum land surface temperature over Iberian Peninsula, ~~Remote. Sens-Basel,~~  
794 ~~11, 2570. Remote Sensing, 11(21), 2570.~~ ~~https://doi.org/10.3390/rs11212570, 2019.~~  
795

796 Kamae, Y., Mei, W., ~~and~~ Xie, S.-P.: ~~(2017)~~. Climatological relationship between warm season  
797 atmospheric rivers and heavy rainfall over East Asia, ~~J. Meteorol. Soc. Jpn., Journal of the~~  
798 ~~Meteorological Society of Japan. Ser. II, 95(6), 411–431. https://doi.org/10.2151/jmsj.2017-027,~~  
799 ~~2017.~~  
800

801 Kenfack, K., Tamoffo, A. T., Djotang Tchotchou, L. A., ~~and~~ Vondou, D. A.: ~~(2023)~~. Assessment  
802 of uncertainties in reanalysis datasets in reproducing thermodynamic mechanisms in the moisture  
803 budget's provision in the Congo Basin, ~~Theor. Appl. Climatol., 154. Theoretical and Applied~~  
804 ~~Climatology, 154(1–2), 613–626. https://doi.org/10.1007/s00704-023-04576-0, 2023.~~  
805

806 Kenfack, K., Tamoffo, A. T., Tchotchou, L. A. D., Marra, F., Kaissassou, S., Nana, H. N., ~~and~~  
807 Vondou, D. A.: ~~(2024)~~. Processes behind the decrease in Congo Basin precipitation during the rainy  
808 seasons inferred from ERA-5 reanalysis, ~~Int. J. Climatol., International Journal of Climatology.~~  
809 ~~https://doi.org/10.1002/joc.8410, 2024.~~  
810

811 ~~Kuete, G., Pokam Mba, W., and Washington, R.: African Easterly Jet South: Control, maintenance~~  
812 ~~mechanisms and link with Southern subtropical waves, Clim. Dynam., 54, 1539–1552,~~  
813 ~~https://doi.org/10.1007/s00382-019-05072-w, 2019.~~

814 ~~Kenya — over 100 dead, 18,000 displaced after recent floods and landslides — floodlist. (n.d.)-~~  
815 ~~Retrieved April 2, 2024, from http://floodlist.com/africa/kenya-floods-november-2019~~  
816

817 [Li, P., Zhou, T., and Chen, X.: Water vapor transport for spring persistent rains over southeastern](#)  
818 [China based on five reanalysis datasets, \*Clim. Dynam.\*, 51, 4243–4257,](#)  
819 <https://doi.org/10.1007/s00382-017-3680-3>, 2017.

820 ~~Kuete, G., Pokam Mba, W., & Washington, R. (2019). African Easterly Jet South: Control,~~  
821 ~~maintenance mechanisms and link with Southern subtropical waves. *Climate Dynamics*,~~  
822 ~~54(3–4), 1539–1552. <https://doi.org/10.1007/s00382-019-05072-w>~~

823

824 [Liu, S., Wen, N., and Li, L.: Dynamic and thermodynamic contributions to Northern China dryness](#)  
825 [in El Niño developing summer, \*Int. J. Climatol.\*, 41, 2878–2890, <https://doi.org/10.1002/joc.6995>,](#)  
826 [2021.](#)

827 ~~Li, P., Zhou, T., & Chen, X. (2017). Water vapor transport for spring persistent rains over~~  
828 ~~southeastern China based on five reanalysis datasets. *Climate Dynamics*, 51(11–12), 4243–~~  
829 ~~4257. <https://doi.org/10.1007/s00382-017-3680-3>~~

830

831 [Longandjo, G.-N. T. and Rouault, M.: Revisiting the seasonal cycle of rainfall over Central Africa, \*J.\*](#)  
832 [Climate, 37, 1015–1032, <https://doi.org/10.1175/jcli-d-23-0281.1>, 2024.](#)

833 ~~Liu, S., Wen, N., & Li, L. (2021). Dynamic and thermodynamic contributions to Northern~~  
834 ~~China dryness in El Niño developing summer. *International Journal of Climatology*, 41(4),~~  
835 ~~2878–2890. <https://doi.org/10.1002/joc.6995>~~

836

837 [Lutz, K., Rathmann, J., and Jacobeit, J.: Classification of warm and cold water events in the eastern](#)  
838 [tropical Atlantic Ocean, \*Atmos. Sci. Lett.\*, 14, 102–106, <https://doi.org/10.1002/asl2.424>, 2013.](#)

839 ~~Longandjo, G.-N. T., & Rouault, M. (2024). Revisiting the seasonal cycle of rainfall over~~  
840 ~~Central Africa. *Journal of Climate*, 37(3), 1015–1032. [https://doi.org/10.1175/jcli-d-23-](https://doi.org/10.1175/jcli-d-23-0281.1)~~  
841 ~~[0281.1](https://doi.org/10.1175/jcli-d-23-0281.1)~~

842

843 ~~Mariotti, L., Diallo, I., Coppola, E., and Giorgi, F.: (2014). Seasonal and intraseasonal changes of~~  
844 ~~African monsoon climates in 21st century CORDEX projections, *Climatic. Climate Change*, 125(1),~~

845 | 53–65, <https://doi.org/10.1007/s10584-014-1097-0>, 2014.

846

847 | Marra, F., Levizzani, V., ~~and~~ Cattani, E.: ~~(2022)~~. Changes in extreme daily precipitation over  
848 Africa: Insights from a non-asymptotic statistical approach, *J. Hydrol. – Journal of Hydrology* X, 16,  
849 100130, <https://doi.org/10.1016/j.hydroa.2022.100130>, 2022.

850

851 | Moon, S. ~~and~~ & Ha, K.-J.: ~~(2020)~~. Future changes in monsoon duration and precipitation using  
852 CMIP6, *NPJ Clim. Atmos. S.*, 3, ~~Npj Climate and Atmospheric Science~~, 3(1).  
853 <https://doi.org/10.1038/s41612-020-00151-w>, 2020.

854

855 | Moudi Pascal, I., Kammalac Jores, T., Talib, J., Appolinaire, V. D., Hirons, L., Christian, N., Tene  
856 Romeo-Ledoux, D., Fogang Michael, T., Marceline, M., Tanessong Roméo, S., Dione, C.,  
857 Thompson, E., Salih, A. A. M., ~~and~~ & Ngaryamgaye, S.: ~~(2023)~~. Strengthening weather forecast and  
858 dissemination capabilities in Central Africa: Case assessment of intense flooding in January 2020,  
859 *Climate Services*, 32, 100411, <https://doi.org/10.1016/j.cliser.2023.100411>, 2023.

860

861 | Nana, H. N., Tanessong, R. S., Tchotchou, L. A. D., Tamoffo, A. T., Moihamette, F., ~~and~~ & Vondou,  
862 D. A.: ~~(2023)~~. Influence of strong South Atlantic Ocean Dipole on the Central African rainfall's  
863 system, *Clim. Dynam.*, 62, ~~Climate Dynamics~~, 62(1), 1–16, [https://doi.org/10.1007/s00382-023-](https://doi.org/10.1007/s00382-023-06892-7)  
864 [06892-7](https://doi.org/10.1007/s00382-023-06892-7), 2023.

865

866 | Neelin, J. D.: ~~(2021)~~. Moist dynamics of tropical convection zones in monsoons, teleconnections,  
867 and global warming, *in: In The Global Circulation of the Atmosphere*, (pp. 267–301). Princeton  
868 University Press, 267–301, 2021. <http://dx.doi.org/10.2307/j.ctv1t1kg52.14>

869

870 | Ngandam Mfondoum, A. H., Wokwenmendiam Nguet, P., Mefire Mfondoum, J. V., Tchindjang, M.,  
871 Hakdaoui, S., Cooper, R., Gbetkom, P. G., Penaye, J., Bekoa, A., ~~and~~ & Moudioh, C.: ~~(2021)~~.  
872 Adapting sudden landslide identification product (SLIP) and detecting real-time increased  
873 precipitation (DRIP) algorithms to map rainfall-triggered landslides in Western Cameroon highlands  
874 (Central-Africa), *Geoenvironmental Disasters*, 8, ~~(1)~~, <https://doi.org/10.1186/s40677-021-00189-9>,  
875 [2021](https://doi.org/10.1186/s40677-021-00189-9).

876

877 | Nicholson, S. E., Fink, A. H., Funk, C., Klotter, D. A., ~~and~~ & Satheesh, A. R.: ~~(2022)~~.  
878 Meteorological causes of the catastrophic rains of October/November 2019 in equatorial Africa,

879 [Global. Planet. ~~Global and Planetary~~ Change, 208, 103687.](#)  
880 <https://doi.org/10.1016/j.gloplacha.2021.103687>, [2022](#).  
881  
882 Oueslati, B., Yiou, P., [and](#) Jézéquel, A.: ~~(2019)~~. Revisiting the dynamic and thermodynamic  
883 processes driving the record-breaking January 2014 precipitation in the southern UK, [Sci. Rep-Uk.](#),  
884 [9](#), ~~Scientific Reports, 9(1)~~. <https://doi.org/10.1038/s41598-019-39306-y>, [2019](#).  
885  
886 [Pokam, W. M., Djiotang, L. A. T., and Mkankam, F. K.: Atmospheric water vapor transport and](#)  
887 [recycling in Equatorial Central Africa through NCEP/NCAR reanalysis data, Clim. Dynam., 38,](#)  
888 [1715–1729, https://doi.org/10.1007/s00382-011-1242-7, 2011.](#)  
889 [Pokam, W. M., Bain, C. L., Chadwick, R. S., Graham, R., Sonwa, D. J., & Kamga, F. M.](#)  
890 [\(2014\). Identification of processes driving low-level westerlies in West Equatorial Africa.](#)  
891 [Journal of Climate, 27\(11\), 4245–4262. https://doi.org/10.1175/jcli-d-13-00490.1](#)  
892  
893 [Pokam, W. M., Bain, C. L., Chadwick, R. S., Graham, R., Sonwa, D. J., and Kamga, F. M.:](#)  
894 [Identification of processes driving low-level westerlies in West Equatorial Africa, J. Climate, 27,](#)  
895 [4245–4262, https://doi.org/10.1175/jcli-d-13-00490.1, 2014.](#)  
896 [Pokam, W. M., Djiotang, L. A. T., & Mkankam, F. K. \(2011\). Atmospheric water vapor](#)  
897 [transport and recycling in Equatorial Central Africa through NCEP/NCAR reanalysis data.](#)  
898 [Climate Dynamics, 38\(9–10\), 1715–1729. https://doi.org/10.1007/s00382-011-1242-7](#)  
899  
900 Seager, R., Naik, N., [and](#) Vecchi, G. A.: ~~(2010)~~. Thermodynamic and dynamic mechanisms for  
901 large-scale changes in the hydrological cycle in response to global warming\*, [J. Journal of Climate,](#)  
902 [23\(17\), 4651–4668. https://doi.org/10.1175/2010jcli3655.1, 2010.](#)  
903  
904 Sheng, B., Wang, H., Li, H., Wu, K., [and](#) Li, Q.: ~~(2023)~~. Thermodynamic and dynamic effects of  
905 anomalous dragon boat water over South China in 2022. [Weather and Climate Extremes, 40,](#)  
906 [100560. https://doi.org/10.1016/j.wace.2023.100560, 2023.](#)  
907  
908 Sonkoué, D., Monkam, D., Fotso-Nguemo, T. C., Yepdo, Z. D., [and](#) Vondou, D. A.: ~~(2018)~~.  
909 Evaluation and projected changes in daily rainfall characteristics over Central Africa based on a

910 multi-model ensemble mean of CMIP5 simulations, *Theor. Appl. Climatol.*, *137*, *Theoretical and*  
911 *Applied Climatology*, *137*(3–4), 2167–2186, <https://doi.org/10.1007/s00704-018-2729-5>, 2018.

912

913 Taguela, T. N., Pokam, W. M., ~~and~~ Washington, R.: ~~(2022)~~. Rainfall in uncoupled and coupled  
914 versions of the Met Office Unified Model over Central Africa: Investigation of processes during the  
915 September–November rainy season, *Int. J. Climatol.*, *42*, *International Journal of Climatology*,  
916 *42*(12), 6311–6331, <https://doi.org/10.1002/joc.7591>, 2022.

917

918 Tamoffo, A. T., Vondou, D. A., Pokam, W. M., Haensler, A., Yepdo, Z. D., Fotso-Nguemo, T. C.,  
919 Tchotchou, L. A. D., ~~and~~ Nouayou, R.: ~~(2019)~~. Daily characteristics of Central African rainfall in  
920 the REMO model, *Theor. Appl. Climatol.*, *137*, *Theoretical and Applied Climatology*, *137*(3–4),  
921 2351–2368, <https://doi.org/10.1007/s00704-018-2745-5>, 2019.

922

923 Tamoffo, A. T., Weber, T., Akinsanola, A. A., ~~and~~ Vondou, D. A.: ~~(2023)~~. Projected changes in  
924 extreme rainfall and temperature events and possible implications for Cameroon’s socio-economic  
925 sectors, *Meteorol. Appl.*, *30*, *Meteorological Applications*, *30*(2), <https://doi.org/10.1002/met.2119>,  
926 2023.

927

928 [Vallès-Casanova, I., Lee, S., Foltz, G. R., and Pelegrí, J. L.: On the Spatiotemporal Diversity of](https://doi.org/10.1029/2020gl087108)  
929 [Atlantic Niño and Associated Rainfall Variability Over West Africa and South America, \*Geophys.\*](https://doi.org/10.1029/2020gl087108)  
930 [\*Res. Lett.\*, \*47\*, <https://doi.org/10.1029/2020gl087108>, 2020.](https://doi.org/10.1029/2020gl087108)

931 ~~Wainwright, C. M., Finney, D. L., Kilavi, M., Black, E., & Marsham, J. H. (2020). Extreme~~  
932 ~~rainfall in East Africa, October 2019–January 2020 and context under future climate change.~~  
933 ~~*Weather*, *76*(1), 26–31. <https://doi.org/10.1002/wea.3824>~~

934

935 [Wainwright, C. M., Finney, D. L., Kilavi, M., Black, E., and Marsham, J. H.: Extreme rainfall in East](https://doi.org/10.1002/wea.3824)  
936 [Africa, October 2019–January 2020 and context under future climate change, \*Weather\*, \*76\*, 26–31,](https://doi.org/10.1002/wea.3824)  
937 <https://doi.org/10.1002/wea.3824>, 2020.

938 ~~Wang, L., & Li, T. (2020). Effect of vertical moist static energy advection on MJO eastward~~  
939 ~~propagation: Sensitivity to analysis domain. *Climate Dynamics*, *54*(3–4), 2029–2039.~~  
940 ~~<https://doi.org/10.1007/s00382-019-05101-8>~~

941

942 [Wang, L. and Li, T.: Effect of vertical moist static energy advection on MJO eastward propagation:](#)  
943 [Sensitivity to analysis domain, \*Clim. Dynam.\*, 54, 2029–2039, \[https://doi.org/10.1007/s00382-019-\]\(https://doi.org/10.1007/s00382-019-05101-8\)](#)  
944 [05101-8, 2020a.](#)

945 [Wang, T., & Li, T. \(2020\). Diagnosing the column-integrated moist static energy budget](#)  
946 [associated with the northward-propagating boreal summer intraseasonal oscillation. \*Climate\*](#)  
947 [Dynamics, 54\(11–12\), 4711–4732. <https://doi.org/10.1007/s00382-020-05249-8>](#)

948

949 [Wang, T. and Li, T.: Diagnosing the column-integrated moist static energy budget associated with](#)  
950 [the northward-propagating boreal summer intraseasonal oscillation, \*Clim. Dynam.\*, 54, 4711–4732,](#)  
951 [https://doi.org/10.1007/s00382-020-05249-8, 2020b.](#)

952 [Wantim, M. N., Ughe, W. G., Kwah, D. C., Bah, T. C., Quinette, N., & Ayonghe, S. N.](#)  
953 [\(2023\). Forensic investigation of the Gouache landslide disaster, Western Region, Cameroon.](#)  
954 [Journal of the Cameroon Academy of Sciences, 19\(3\), 223–240.](#)  
955 [https://doi.org/10.4314/jcas.v19i3.3](#)

956

957 [Wantim, M. N., Ughe, W. G., Kwah, D. C., Bah, T. C., Quinette, N., and Ayonghe, S. N.: Forensic](#)  
958 [investigation of the Gouache landslide disaster, Western Region, Cameroon, \*Journal of the\*](#)  
959 [Cameroon Academy of Sciences, 19, 223–240, <https://doi.org/10.4314/jcas.v19i3.3>, 2023.](#)

960 [Washington, R., James, R., Pearce, H., Pokam, W. M., & Moufouma-Okia, W. \(2013\). Congo](#)  
961 [Basin rainfall climatology: Can we believe the climate models? \*Philosophical Transactions of\*](#)  
962 [the Royal Society B: Biological Sciences, 368\(1625\), 20120296.](#)  
963 [https://doi.org/10.1098/rstb.2012.0296](#)

964

965 [Washington, R., James, R., Pearce, H., Pokam, W. M., and Moufouma-Okia, W.: Congo Basin](#)  
966 [rainfall climatology: Can we believe the climate models?, \*Philos. T. R. Soc. B.\*, 368, 20120296,](#)  
967 [https://doi.org/10.1098/rstb.2012.0296, 2013.](#)

968 [Wen, N., Liu, S., & Li, L. Z. X. \(2022\). Diagnosing the dynamic and thermodynamic effects](#)  
969 [for the exceptional 2020 summer rainy season in the Yangtze River Valley. \*Journal of\*](#)

970 | *Meteorological Research*, 36(1), 26–36. <https://doi.org/10.1007/s13351-022-1126-2>

971 |

972 | Wen, N., Liu, S., and Li, L. Z. X.: Diagnosing the dynamic and thermodynamic effects for the  
973 | exceptional 2020 summer rainy season in the Yangtze River Valley, *J. Meteorol. Res-Proc.*, 36, 26–  
974 | 36, <https://doi.org/10.1007/s13351-022-1126-2>, 2022.

975 | Yanai, M., & Tomita, T. (1998). Seasonal and interannual variability of atmospheric heat  
976 | sources and moisture sinks as determined from NCEP–NCAR reanalysis. *Journal of Climate*,  
977 | 11(3), 463–482. [https://doi.org/10.1175/1520-0442\(1998\)011<0463:saivoa>2.0.co;2](https://doi.org/10.1175/1520-0442(1998)011<0463:saivoa>2.0.co;2)

978 |

979 | Yanai, M. and Tomita, T.: Seasonal and interannual variability of atmospheric heat sources and  
980 | moisture sinks as determined from NCEP–NCAR reanalysis, *J. Climate*, 11, 463–482,  
981 | [https://doi.org/10.1175/1520-0442\(1998\)011<0463:saivoa>2.0.co;2](https://doi.org/10.1175/1520-0442(1998)011<0463:saivoa>2.0.co;2), 1998.

982 | Zhao, D., Zhang, L., & Zhou, T. (2022). Detectable anthropogenic forcing on the long-term  
983 | changes of summer precipitation over the Tibetan Plateau. *Climate Dynamics*, 59(7–8), 1939–  
984 | 1952. <https://doi.org/10.1007/s00382-022-06189-1>

985 |

986 | Zhao, D., Zhang, L., and Zhou, T.: Detectable anthropogenic forcing on the long-term changes of  
987 | summer precipitation over the Tibetan Plateau, *Clim. Dynam.*, 59, 1939–1952,  
988 | <https://doi.org/10.1007/s00382-022-06189-1>, 2022.

989 | Zhou, L., Tian, Y., Myneni, R. B., Ciais, P., Saatchi, S., Liu, Y. Y., Piao, S., Chen, H.,  
990 | Vermote, E. F., Song, C., & Hwang, T. (2014). Widespread decline of Congo rainforest  
991 | greenness in the past decade. *Nature*, 509(7498), 86–90. <https://doi.org/10.1038/nature13265>

992 |

993 | Zhou, L., Tian, Y., Myneni, R. B., Ciais, P., Saatchi, S., Liu, Y. Y., Piao, S., Chen, H., Vermote, E.  
994 | F., Song, C., and Hwang, T.: Widespread decline of Congo rainforest greenness in the past decade,  
995 | *Nature*, 509, 86–90, <https://doi.org/10.1038/nature13265>, 2014.

996 |